Department for
Business, Energy
& Industrial Strategy

Primary Store Geophysical Model & Report

Key Knowledge Document

NS051-SS-REP-000-00013

August 2021

Acknowledgements

Any enquiries regarding this publication should be sent to us at:
enquiries@beis.gov.uk

Contents

Terms and Abbreviations

2D	Two-dimensional (seismic survey)
2DHR	Two-dimensional High Resolution (seismic survey)
3D	Three-dimensional (seismic survey)
AI	Acoustic Impedance
BCU	Base Cretaceous Unconformity
BEIS	Department of Business, Energy and Industrial Strategy
Capture	Collection of CO_2 from power station combustion process or other facilities and its process ready for transportation
Carbon	An element, but used as shorthand for its gaseous oxide, CO_2
CCGT	Combined Cycle Gas Turbine
CCUS	Carbon Capture, Utilisation and Storage
CO_2	Carbon Dioxide
DST	Drill Stem Test
FEED	Front-End Engineering Design
FFM	Full Field Model
FID	Final Investment Decision
GRV	Gross Rock Volume
HC	Hydrocarbon
HMG	Her Majesty's Government (UK government)
Key Knowledge	Information that may be useful, if not vital, to understanding how some enterprise may be successfully undertaken
MDT	Modular Formation Dynamic Tester
MM	Million
MMV	Monitoring, Measurement, and Verification
MT	Mega Tonne (10^6 metric tonnes)
MTPA	Mega Tonnes per Annum
NEP	Northern Endurance Partnership
NPV	Net Pore Volume
NUI	Normally Unmanned Installation
NZT	Net Zero Teesside
OBC	Ocean Bottom Cable
SCAL	Special Core Analysis
SNS	Southern North Sea
SPB	Southern Permian Basin
SPR	Seismic Phase Reversal
Storage	Containment in suitable pervious rock formations located under impervious rock formations usually under the seabed
TDRM	Top-Down Reservoir Modelling
TDS	Total Dissolved Solids
Transport	Removing processed CO_2 by pipeline from the capture and process unit to storage
TVDSS	True Vertical Depth Subsea
TWT	Two-way Time
UKCS	United Kingdom Continental Shelf
ZCH	Zero Carbon Humberside

Foreword

The Net Zero Teesside (NZT) project in association with the Northern Endurance Partnership project (NEP) intend to facilitate decarbonisation of the Humber and Teesside industrial clusters during the mid-2020s. Both projects will look to take a Final Investment Decision (FID) in early 2023, with first CO2 capture and injection anticipated in 2026.

The projects address widely accepted strategic national priorities – most notably to secure green recovery and drive new jobs and economic growth. The Committee on Climate Change (CCC) identified both gas power with Carbon Capture, Utilisation and Storage (CCUS) and hydrogen production using natural gas with CCUS as critical to the UK's decarbonisation strategy. Gas power with CCUS has been independently estimated to reduce the overall UK power system cost to consumers by £19bn by 2050 (compared to alternative options such as energy storage).

Net Zero Teesside Onshore Generation & Capture

NZT Onshore Generation & Capture (G&C) is led by bp and leverages world class expertise from ENI, Equinor, and TotalEnergies. The project is anchored by a world first flexible gas power plant with CCUS which will compliment rather than compete with renewables. It aims to capture ~2 million tonnes of CO2 annually from 2026, decarbonising 750MW of flexible power and delivering on the Chancellor's pledge in the 2020 Budget to "support the construction of the UK's first CCUS power plant." The project consists of a newbuild Combined Cycle Gas Turbine (CCGT) and Capture Plant, with associated dehydration and compression for entry to the Transportation & Storage (T&S) system.

Northern Endurance Partnership Onshore/Offshore Transportation & Storage

The NEP brings together world-class organisations with the shared goal of decarbonising two of the UK's largest industrial clusters: the Humber (through the Zero Carbon Humber (ZCH) project), and Teesside (through the NZT project). NEP T&S includes the G&C partners plus Shell, along with National Grid, who provide valuable expertise on the gathering network as the current UK onshore pipeline transmission system operator.

The Onshore element of NEP will enable a reduction of Teesside's emissions by one third through partnership with industrial stakeholders, showcasing a broad range of decarbonisation technologies which underpin the UK's Clean Growth strategy and kickstarting a new market for CCUS. This includes a new gathering pipeline network across Teesside to collect CO2 from industrial stakeholders towards an industrial Booster Compression system, to condition and compress the CO2 to Offshore pipeline entry specification.

Offshore, the NEP project objective is to deliver technical and commercial solutions required to implement innovative First-of-a-Kind (FOAK) offshore low-carbon CCUS infrastructure in the UK, connecting the Humber and Teesside Industrial Clusters to the Endurance CO2 Store in the Southern North Sea (SNS). This includes CO2 pipelines connecting from Humber and Teesside compression/pumping systems to a common subsea manifold and well injection site

at Endurance, allowing CO2 emissions from both clusters to be transported and stored. The NEP project meets the CCC's recommendation and HM Government's Ten Point Plan for at least two clusters storing up to 10 million tonnes per annum (Mtpa) of CO2 by 2030.

TEESSIDE (NZT)

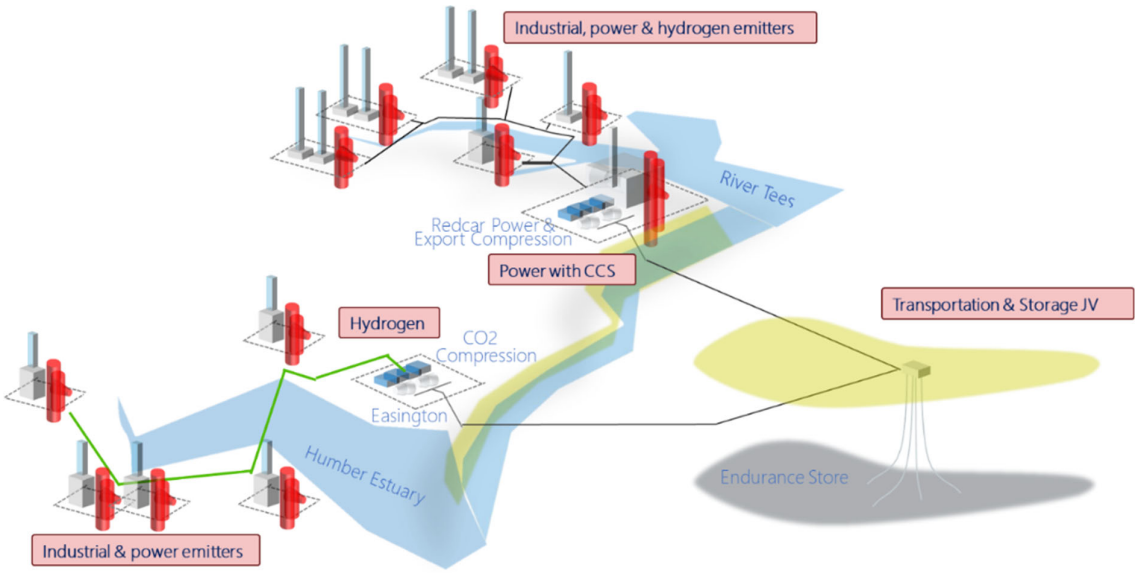

HUMBERSIDE (ZHC) NEP

The project initially evaluated two offshore CO2 stores in the SNS: 'Endurance', a saline aquifer formation structural trap, and 'Hewett', a depleted gas field. The storage capacity requirement was for either store to accept 6+ Mtpa CO2 continuously for 25 years. The result of this assessment after maturation of both options, led to Endurance being selected as the primary store for the project. This recommendation is based on the following key conclusions:

The storage capacity of Endurance is 3 to 4 times greater than that of Hewett

The development base cost for Endurance is estimated to be 30 to 50% less than Hewett

CO2 injection into a saline aquifer is a worldwide proven concept, whilst no benchmarking is currently available for injection in a depleted gas field in which Joule-Thompson cooling effect has to be managed via an expensive surface CO2 heating solution.

Following selection of Endurance as the primary store, screening of additional stores has been initiated to replace Hewett by other candidates. Development scenarios incorporating these additional stores will be assessed as an alternative to the sole Endurance development.

Executive Summary

The Endurance structure has been geophysically assessed and interpreted, along with well calibrations and seismic rock property modelling studies, to characterise the subsurface and define the structural framework. Several seismic datasets were available (2D of varying vintages, 1997 ocean-bottom-cable 3D and 2013 Polarcus towed-streamer 3D), which in combination provided coverage of the Endurance structure and the outcrop to southeast. However, the existing seismic had limitations with fold and noise due to processing for deeper pre-salt targets. A reprocessing of the 2013 Polarcus 3D was undertaken specifically for this project, which significantly enhanced the image quality and reduced the noise within the dataset, enabling improved confidence in horizon and fault interpretation over the Endurance structure and outcrop.

Interpretation on the new dataset results in a very similar two-way time structure of Endurance. The Top Bunter Sandstone is a very clear seismic event, and the seismic phase reversal is highly visible in all attributes. However, low impedance contrasts within the reservoir section mean that derivation of seismic attributes for reservoir characterisation has not been possible. The Top Bunter Shale (base reservoir) horizon was additionally interpreted, which had not been possible previously.

The overburden stratigraphy over Endurance is conformable and generally isopachous and the seismic character is very consistent. No evidence of an angular unconformity exists within the Triassic or Lias section, therefore, the earliest the Endurance structure could have grown was the late Cretaceous.

Faults were mapped in the overburden on the new reprocessed 2013 Polarcus 3D seismic data, down to a resolution of around 15m. Two main trends were observed - NW-SE over the crest of the Endurance anticline, and roughly E-W trending faults to the east of the Endurance structure. No faulting is observed within the reservoir section on the Endurance structure, although some minor sub-seismic faulting is likely to exist.

The seismic data and interpretations were depth converted using a simple layered model (V0k). The depth converted horizons and faults provided the structural framework input to the static reservoir model and geomechanical models, as well as upside and downside scenarios of depth structure and fault transmissibility to test uncertainty.

The 4D seismic response from CO2 injection is predicted to be very good. CO2 will be detectable even at very low saturations, although the seismic is less sensitive to the volume of CO2, which will limit overall plume monitoring and management.

The existing seismic data, even after reprocessing, is not optimal for the Bunter Sandstone at Endurance. It is recommended to acquire a new high resolution 3D seismic, with improved spatial sampling and noise removal, focussed on the CO2 store. A depth migration will decrease any depth errors in structure and spill point ahead of well planning. High resolution coverage over the 42/25d-3 appraisal well will also help facilitate well-tie to core and improve seismic reservoir characterisation.

1.0 Introduction

The Endurance structure in the Southern North Sea is one of several saline aquifer structures that have been identified as potentially suitable storage sites for CCUS. This report is one of a series of key knowledge documents (KKD), which describes the work program undertaken by the Net Zero Teesside & Northern Endurance Partnership (NZT/NEP) to characterise the subsurface at Endurance and create subsurface models for evaluation of CO2 injection and storage at the Endurance CO2 store.

1.1 Purpose

The purpose of this document is to summarize the work program completed on geophysical aspects of the integrated subsurface description of the Endurance store. This follows previous studies such as those completed as part of the White Rose project. Early analysis of previous studies highlighted a number of key areas to further advance understanding, which were drawn together and used in the development of the geophysical model used to test subsurface uncertainties and assess risk.

Subsurface storage risks can be broadly classified as those relating to containment, capacity, injectivity and monitorability, with those covered by this document focussing on containment, capacity and monitorability. Key areas to advance geophysical understanding to assess containment, capacity and monitorability uncertainties and risks at the Endurance store were identified as:

Regional geology – the tectonic history of the basin, general depositional environment and variation of the Bunter Sandstone at a regional scale, diagenetic effects on brine aquifer connectivity, regional seals, analogues in the wider Southern North Sea and the petroleum charge history of the basin

Structural understanding of the container/trap – development of the Endurance structure, assessing container dimension uncertainty, understanding of present day stresses and inputs for the geomechanical integrity study

Faulting and assessment of any compartmentalisation – interpretation of overburden faulting and lack of faulting through store seals, assessment of any faulting within the reservoir, use of structural analogues and characterisation of scenarios to test transmissibility and compartmentalisation of the reservoir

These were investigated via geophysical assessment and interpretation of the seismic data over the Endurance structure, along with well calibrations and seismic rock property modelling studies.

1.2 Location

The Endurance CO2 store is situated within the United Kingdom Continental Shelf (UKCS) in the Southern North Sea (SNS), about 75 km east offshore from Flamborough Head (**Figure 1**). It straddles blocks 42/25 and 43/21 and the water depth is around 50 m. The depth to the

structural crest at the top CO2 injection interval (Bunter Sandstone Formation) is about 1000 mTVDSS.

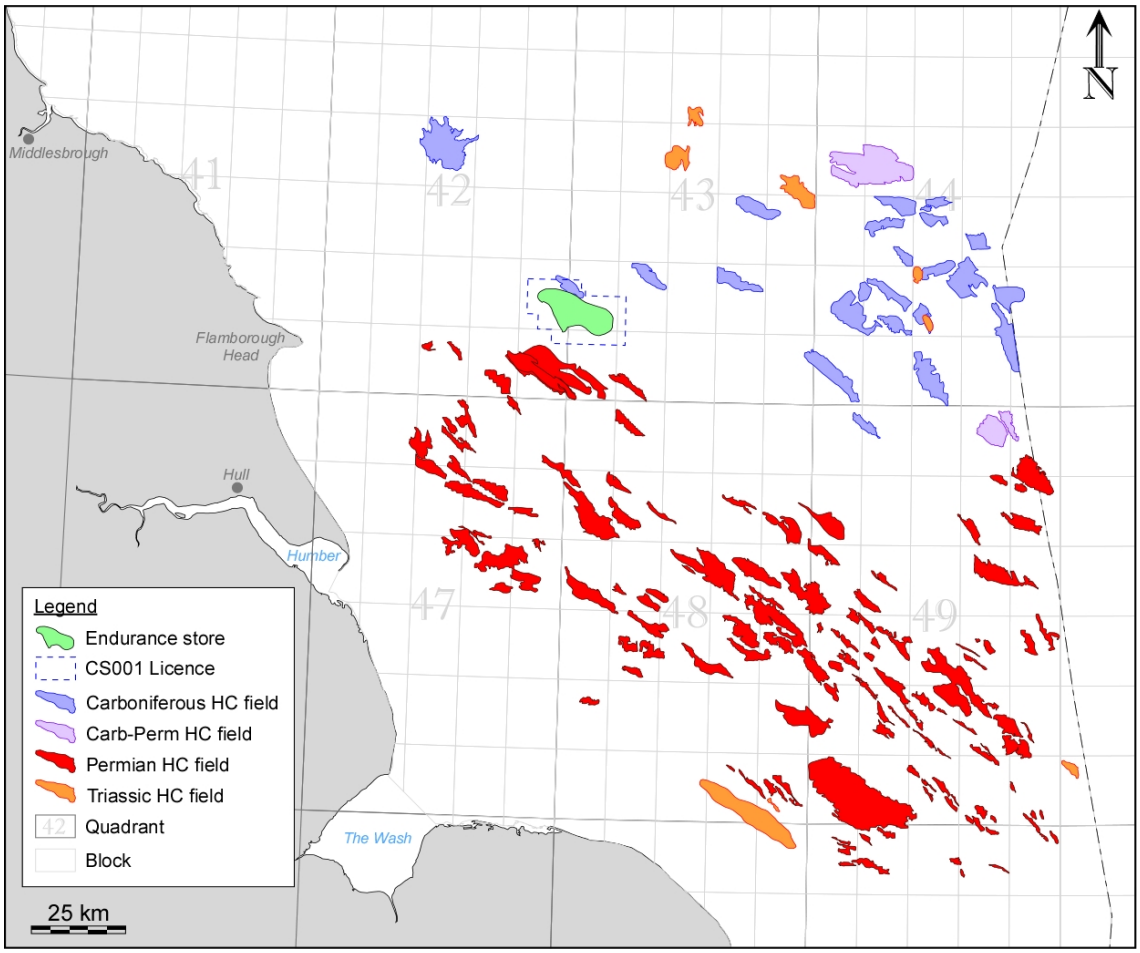

Figure 1 - Location map of the Endurance CO2 store in the Southern North Sea.

1.3 Geological Setting

The Endurance structure is a large, four-way dip-closed anticline, formed above a salt pillow, approximately 25 km long by 8 km wide, oriented NW–SE. It is located within the Silverpit sub-basin at the western end of the much larger, E–W striking Southern Permian Basin (SPB). The basin is bound to the west by the Dowsing Fault Zone and to the east by the Cleaver Bank High. The northern limit is defined by the Mid North Sea High and the southern limit by the London-Brabant Massif (**Figure 2**).

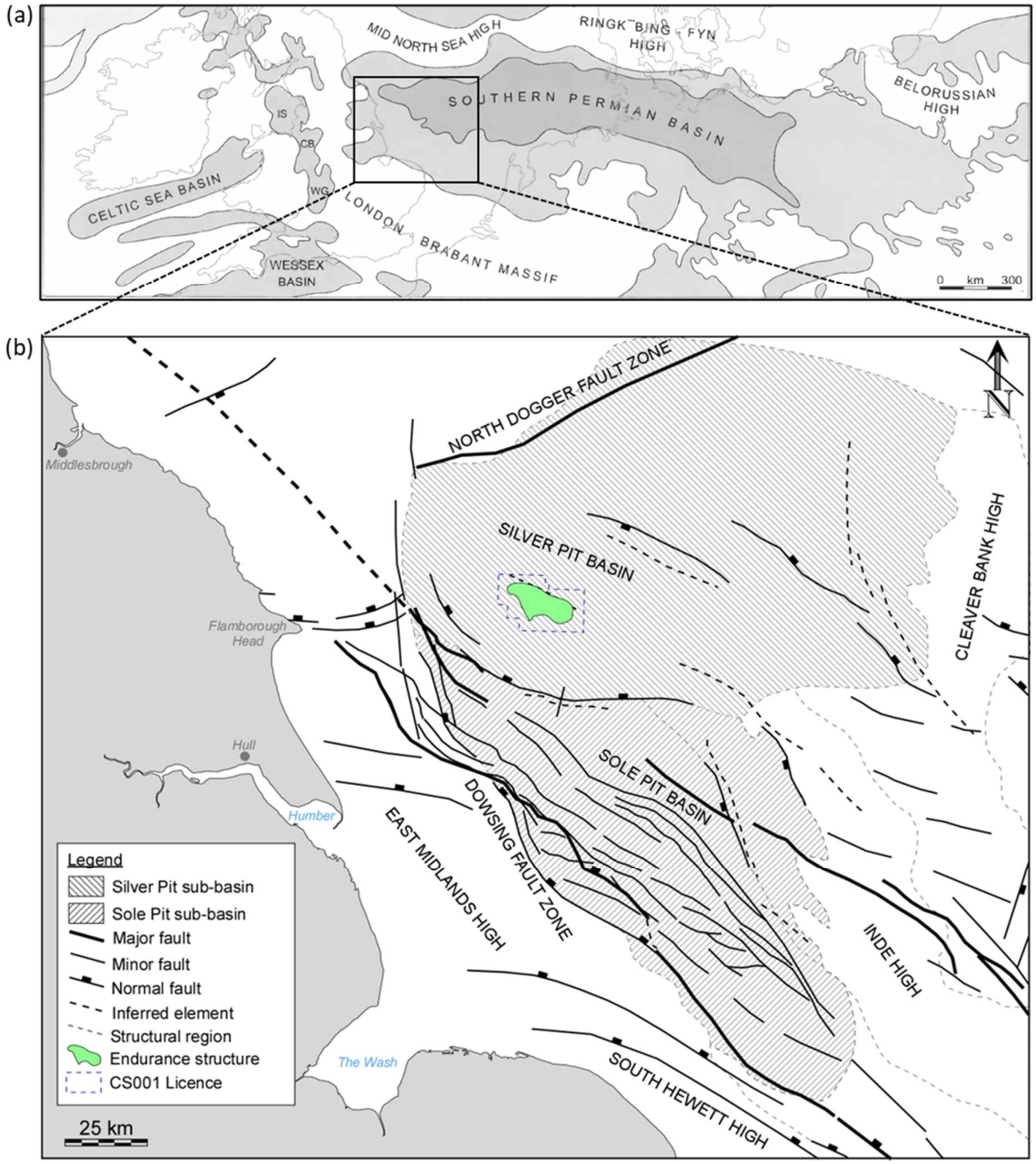

Figure 2 – Tectonic setting: (a) Extent of the Southern Permian Basin (modified from Underhill, 2003); (b) Structural elements of the Southern North Sea (modified from Richards, 2015; Pharoah et al., 2010).

1.3.1 Structural and Stratigraphic Evolution

The region has had a complex tectonic evolution but can be summarised into three key evolutionary periods: Palaeozoic continental collision and plate accretion (formation of Pangea), late Palaeozoic–Mesozoic intraplate subsidence and continental rift tectonics (break-up of Pangea), and late Mesozoic–Cenozoic inversion and thermal uplift (Alpine Collision). The regional tectonostratigraphy of the SNS is summarised in **Figure 3** and the lithostratigraphy is summarised in **Figure 4**. The oldest sediments penetrated within the Endurance area are those deposited during the mid to late Carboniferous, unconformably

overlain by a thick sequence of Permian, Triassic and early Jurassic sediments. A major unconformity separates the Jurassic from the Cretaceous to Cenozoic stratigraphy.

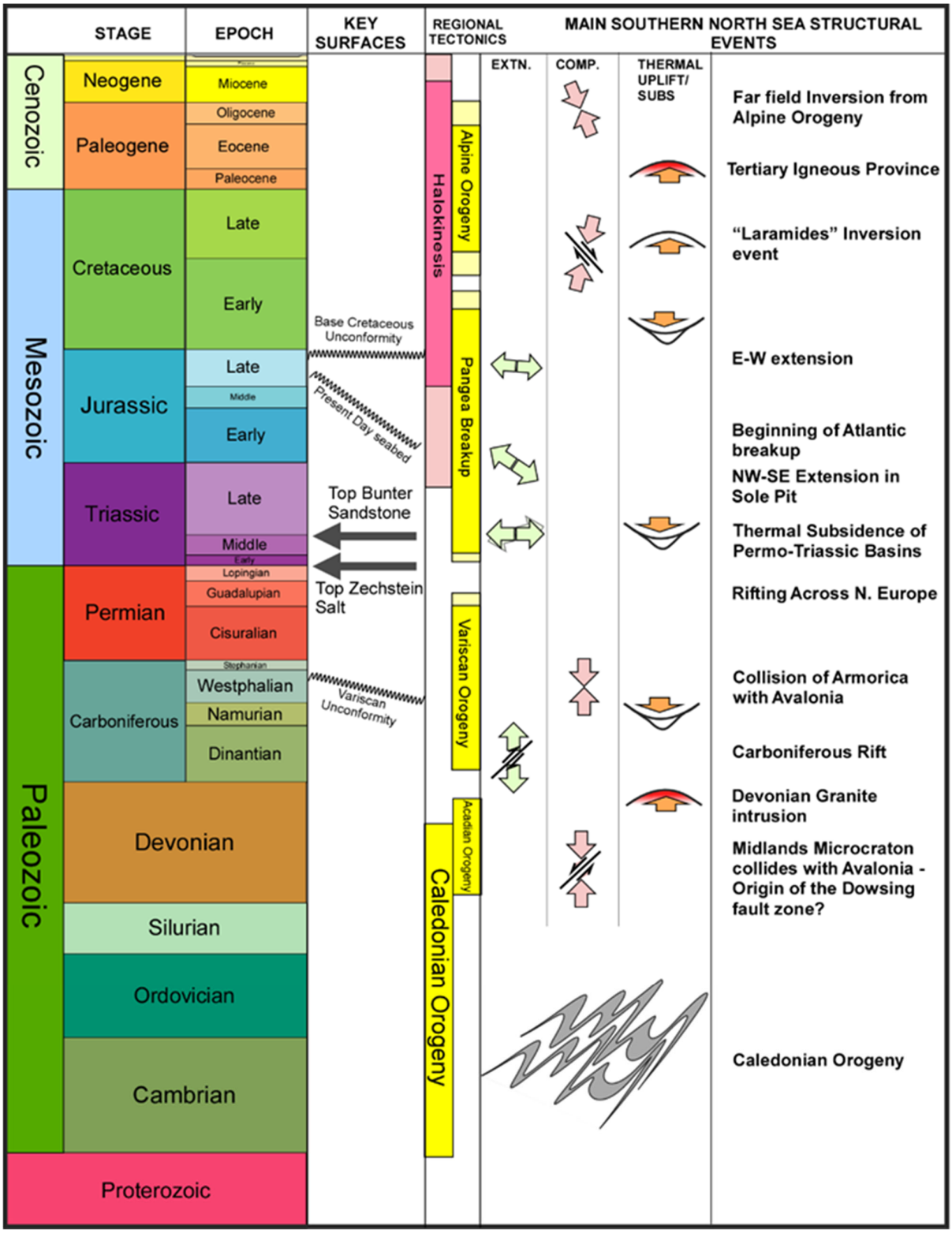

Figure 3 - Regional tectonostratigraphy of the Southern North Sea.

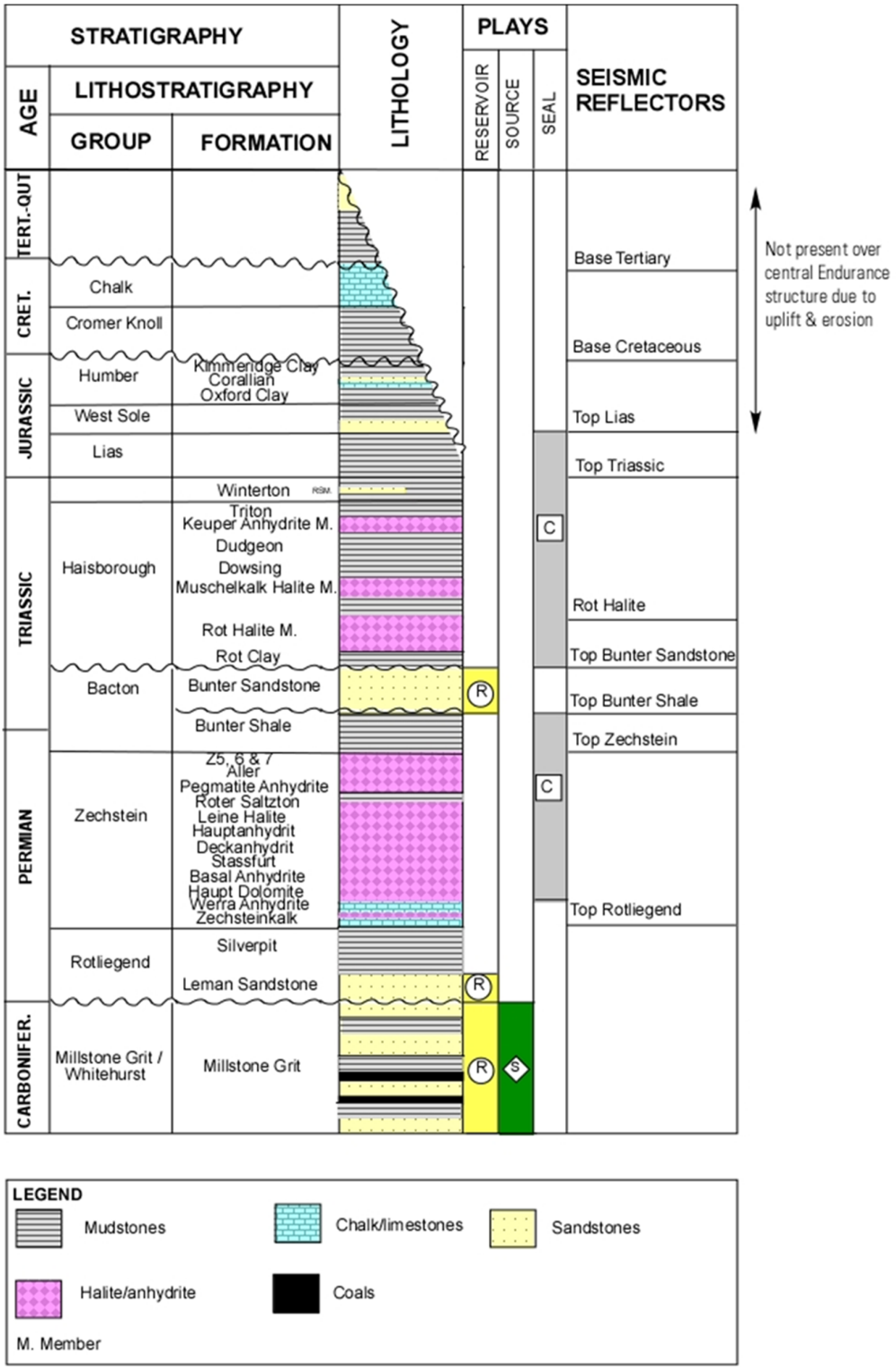

Figure 4 - Stratigraphic column for the Southern North Sea.

1.3.1.1 Ordovician to Carboniferous

Much of the structural fabric originates from the Caledonian and Variscan plate tectonic cycles during the Palaeozoic (Underhill, 2003). The Ordovician to Devonian Caledonian Orogeny influenced the development of NW–SE striking structures aligned with the northeastern boundary of the Midlands Microcraton during the Devonian (e.g. the Dowsing Fault Zone) (Guterch et al., 2010). Lithospheric extension and rifting commenced during the late Devonian to early Carboniferous, with active fault-bounded half grabens and tilted fault blocks developed in the Southern North Sea area, following the NW–SE trends of the older Caledonian basement (Coward et al., 2003; Moscariello, 2003). By the Late Carboniferous, the Southern North Sea area had transitioned to humid equatorial conditions and was an established deltaic province, characterised by deltaic to fluvio-lacustrine deposits with numerous coal layers (Underhill, 2003; Kombrink et al., 2010). Subsequent compression associated with the Variscan Orogeny resulted in fault reactivation, folding, uplift and erosion of the Carboniferous strata, with progressively younger Carboniferous-age rocks sub-cropping from west to east beneath the Variscan Unconformity (Moscariello, 2003; Grant et al., 2018).

1.3.1.2 Permian

Subsidence in the early Permian, in response to post-orogenic collapse and rifting at the end of the Variscan Orogeny, led to the development of the intracratonic Southern Permian Basin. This was an extensive basin which extended from the UK Southern North Sea eastwards as far as Poland (Underhill, 2003; Grant et al., 2018). Syn-sedimentary rifting occurred during the Permian, influenced by the NW–SE basement fault trends, which continued to be reactivated repeatedly during the Mesozoic and Cenozoic.

The ongoing plate tectonic movements meant that by the time the Southern Permian Basin was initiated it had drifted northwards of the equator to within the northern hemisphere desert belt (Glennie, 1997). An arid climate prevailed and the Permian Rötliegend Group deposition was within an entirely land-locked basin, with terminal playa and saline lakes developed in the central, deepest parts of the basin. Within the Southern North Sea area, the Rötliengend Group is represented by two key formations: the Leman Sandstone Formation and the Silverpit Formation. The Leman Sandstone Formation consists of cross-bedded, dune sandstones deposited within an aeolian desert environment, which laterally grade northwards into the Silverpit Formation, composed of mudstones and interbedded evaporites deposited within a playa lake environment (Gast et al., 2010; Underhill, 2003).

The Southern Permian Basin was flooded by marine waters during the late Permian. The Zechstein Group depositional environment reflects cycles of marine incursions which subsequently increased in salinity and progressively evaporated, leading to cyclic deposition of marine carbonates and mudstones followed by widespread evaporite deposits (Glennie, 1997; Underhill, 2003).

1.3.1.3 Triassic

The active basin extension in the Southern North Sea area waned through the late Permian and was succeeded by a phase of thermal subsidence, a period of tectonic quiescence which

continued through the Triassic to Early Jurassic times (Underhill, 2003; Grant et al., 2018). Semi-arid continental conditions also returned at the end of the Permian. Ephemeral fluvial systems drained northwards off the Variscan fold belt and the Triassic Bacton Group sediments (Bunter Shale Formation and Bunter Sandstone Formation) were deposited in predominantly fluvial, lacustrine and playa lake environments, which were subject to aeolian reworking (Bachmann et al.,2010; Geluk et al, 2018). In the mid Triassic, episodic marine incursions into partially restricted basins under dry climatic conditions resulted in the deposition of marine (and subordinate lacustrine) evaporites, mudstones and limestones of the lower Haisborough Group (Geluk et al;, 2018; Moscariello, 2003). In the late Triassic, more non-marine conditions returned, with deposition of clastics, evaporites and carbonates in emphemeral lake and fluvial systems (upper Haisborough Group). At the end of the Triassic (Penarth Group), there was a marine transgression and the depositional environments transitioned from non-marine, through paralic systems to marine conditions by the early Jurassic (Bachmann et al., 2018).

Subsidence in the Triassic–Jurassic was controlled by continued extension on the Dowsing Fault Zone, but sediment distribution was increasingly affected by salt tectonics, whereby the Zechstein Salt that had been deposited during the Late Permian formed into salt swells in response to the developing sedimentary load (Stewart & Coward, 1995; Pharaoh et al., 2010).

1.3.1.4 Jurassic to Early Cretaceous

Global sea level rise and flooding in the early Jurassic created a shallow epicontental basin into which shallow, open-marine, fine-grained mudstones of the Lias Group were deposited (Lott et al., 2010). In the mid Jurassic, thermal doming and uplift in the region of the North Sea Rift triple junction to the north of the Southern North Sea led to considerable erosion and removal of much of the Mesozoic section (Stewart & Coward, 1995; Pharaoh et al., 2010). The subsequent collapse of the thermal dome culminated in the extensional tectonics of the North Sea Rift during the Late Jurassic to Early Cretaceous, which was expressed as transtensional subsidence in NW-SE trending Sole Pit Basin, whilst rift flank uplift and erosion took place to the northeast, resulting in a combined complex of unconformities known as the Base Cretaceous Unconformity (Stewart & Coward, 1995; Pharaoh et al., 2010; Grant et al., 2018). The remainder of the Jurassic section after the Lias Group is absent in the area of interest due to the erosion associated with the Base Cretaceous Unconformity.

1.3.1.5 Late Cretaceous to Cenozoic

Open-marine depositional environments continued throughout the Cretaceous, with the deposition of shallow-marine argillaceous sediments of the Cromer Group in the Lower Cretaceous, followed by a thick sequence of chert-rich limestones, chalks and marls of the Chalk Group in the Upper Cretaceous (Moscariello, 2003). Post-rift thermal subsidence was established over the Southern North Sea area by the Late Cretaceous. Towards the end of the Late Cretaceous and throughout the Early Cenozoic, there was widespread basin uplift and several pulses of structural inversion related to the opening of the Atlantic Ocean and Alpine collision in Europe (Pharaoh et el, 2010; Grant et al., 2018). Within the Silverpit Basin, the structure is dominated by NW-trending Zechstein Salt pillows and walls, folding the post-

Permian sequence into a series of NW-SE trending anticlines and synclines. Widespread halokinesis of the Zechstein salts was triggered by the Cenozoic inversion and reactivation of basement faults under a dextral transpressional regime (Pharaoh et al., 2010; Conway & Valvatne, 2003; Moscariello, 2003). The final phase of inversion was in the Oligocene–Miocene, after which time thermal subsidence resumed and the remainder of the Cenozoic is characterised by marine and glacio-marine argillaceous sandstones, siltstones and clays (O'Mara et al., 2003; Moscariello, 2003).

1.4 Exploration and Appraisal History

Exploration for hydrocarbons first commenced in the Southern North Sea in the 1960s, targeting possible gas at the Triassic Bunter Sandstone 4-way structural closures. This led to the Endurance reservoir being discovered by well 43/21-1, drilled by Mobil in 1970 at the crest of Endurance, which found very saline brine. A suite of conventional logs was run, and the well was abandoned. A second well was drilled by BP in 1990, 42/25-1, targeting the deeper stratigraphy, and confirmed water-bearing at the Triassic Bunter Sandstone interval. Well 42/25d-3 was drilled by National Grid Carbon in 2013 as an appraisal well for the White Rose CO2 storage project, gathering valuable data including 190m of core.

1.5 Storage Site and Storage Complex

The proposed CO2 injection reservoir is the Triassic-age Bunter Sandstone Formation within the structural closure of the Endurance anticline (Storage Site). Containment is provided by the overlying Röt Clay and Röt Halite (base Haisborough Group) as primary seals, plus secondary seals within the remainder of the Haisborough Group, Penarth Group and Early Jurassic. The Storage Complex is defined as the Bunter Sandstone Formation reservoir and overlying Röt Clay, Röt Halite and other seals up to the Jurassic Lias Group, within the structural closure of the Endurance anticline and extending southeast to include the 'outcrop' (a region where the Bunter Sandstone Formation has been folded up to outcrop at seabed due to an underlying Zechstein salt diapir). The Storage Site and Storage Complex are shown in **Figure 5** and the key characteristics are summarised in **Table 1**.

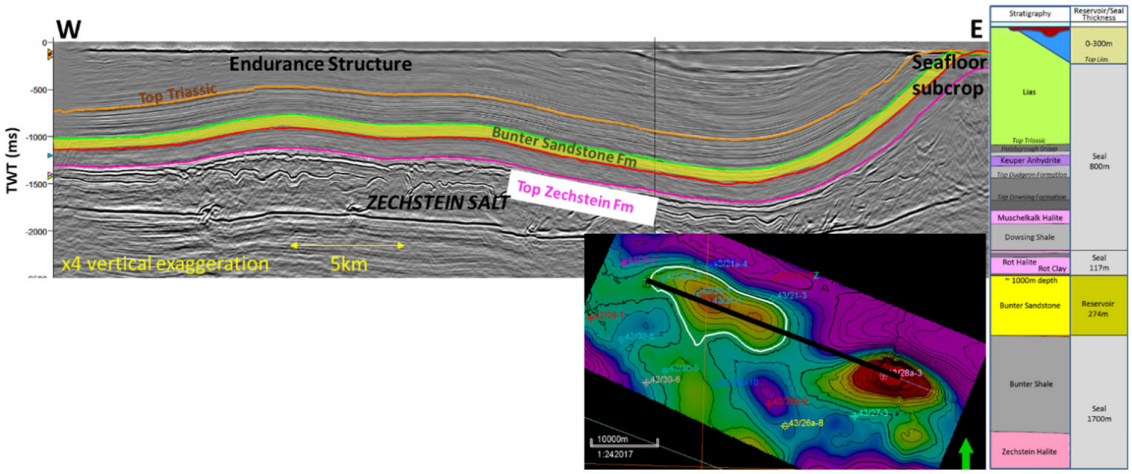

Figure 5 - Endurance storage complex.

Table 1 - Summary of key characteristics of the Endurance CO2 store.

Parameter		Units	Value / Comment
Reservoir	Formation		Bunter Sandstone Formation
	Age		Triassic (Bacton Group)
	Type		Fluvial-aeolian sandstones
	Average thickness	m	275
	Average net to gross	%	94
	Average porosity	%	22.5
	Average permeability	mD	300
	Average salinity	ppm	250,000
Trap	Type		Four-way dip closed anticline
	Depth to crest	mTVDSS	1000
	Spill point	mTVDSS	1450
	Area	km2	140
Seal	Formation		Röt Clay and Röt Halite
	Age		Triassic (Haisborough Group)
	Type		Playa lake mudstones & evaporites
	Thickness	m	110: Röt Clay 10 + Röt Halite 100
Reservoir conditions	Datum depth	mTVDSS	1300
	Initial pressure at datum depth	Psi	2030
	Temperature at datum depth	°C	57

2.0 Seismic Database

The Endurance area is covered by three main seismic datasets (**Figure 6**):

1. 2D seismic (of various vintages)
2. 1997 Ravenspurn ocean-bottom-cable (OBC) 3D seismic survey (herein referred to as 1997 OBC)
3. 2013 Polarcus West and Greater Ravenspurn towed-streamer 3D seismic survey (herein referred to as 2013 Polarcus)

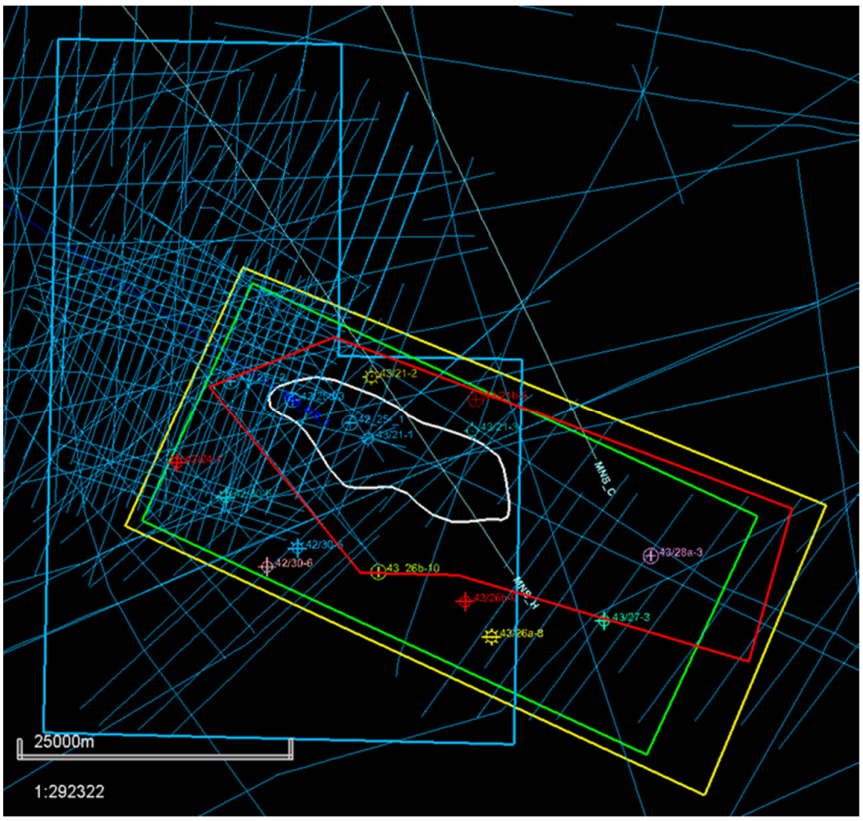

Figure 6 - Seismic coverage over Endurance (white outline is structural closure, yellow rectangle is AOI for this project): 1997 OBC coverage shown by thick blue outline, 2013 Polarcus 3D coverage (purchased for this project) in red outline. Other blue lines are 2D data.

2.1 2D Seismic

The resolution of the better quality 2D seismic data is similar to the quality of the 3D seismic (**Figure 7**). The map in **Figure 6** shows that 2D coverage is not even across the structure, however, for regional understanding of the basin the 2D seismic data is very useful. Where the Zechstein salt becomes more complicated inboard of Endurance (to the southwest) the 2D seismic data is poor (**Figure 7**).

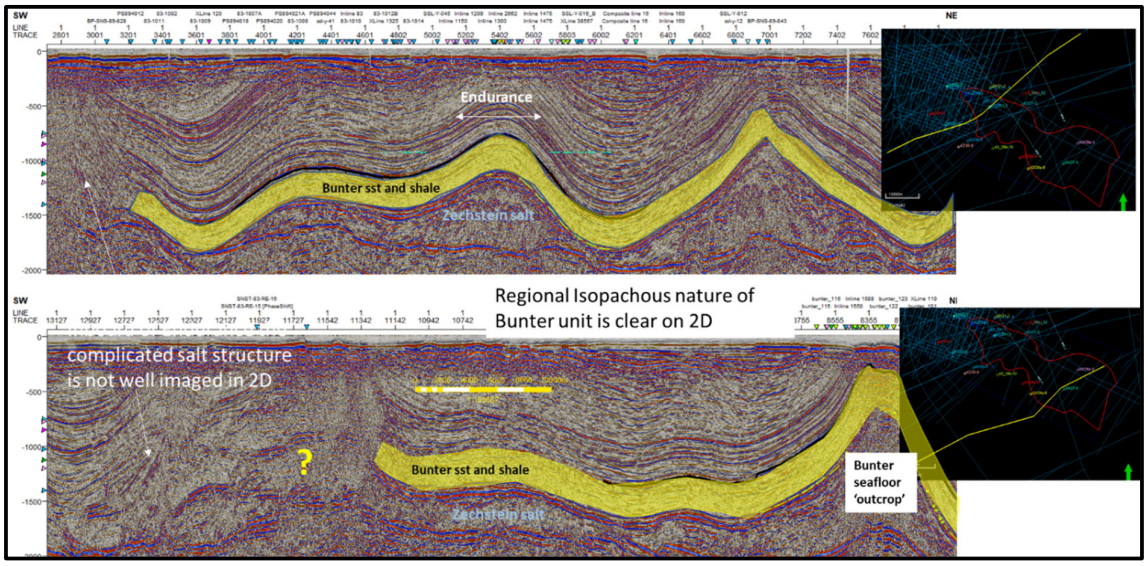

Figure 7 - Examples of 2D lines running SW-NE across the structure and outcrop.

2.2 1997 OBC 3D Seismic

This is a sparse OBC dataset but provides clear structural imaging of Endurance. The acquisition specifications for this survey are shown in **Table 2**. This data has two important deficiencies: there is no coverage of the Bunter Sandstone Formation outcrop to the SE of the Endurance structure (**Figure 6**) and the overburden coverage is very low fold so comprehensive overburden fault interpretation is not possible (**Figure 8**). The low fold of the Bunter Sandstone Formation also prohibits any seismic reservoir characterisation or attribute analysis.

Table 2 - Acquisition specifications for the 1997 OBC 3D seismic survey.

Survey 'Z' Ravenspurn OBC

Acquisition	
Year	1997 (Party 82) and 1998 (Party 66)
Contractor	Western Geophysical
Main Vessel	R/V's Northern Horizon + Chouest Cadet
Source	
Type	Split Areal Sleeve gun array
Number of sources	1
Configuration	Orthogonal shooting, shot lines E-W
Shot line separation	300m
Shot line length	Up to 3.36km
Shot points/line	112
Array depth	5m
Array capacity	1500 cu. In.
Shot interval	30m
Receiver	
Receiver Type	Dual Sensor SH4 (Hydrophone), SM4UB (geo)
Configuration	4 lines of 100 dual sensors per swath
Group Interval	60m
Receiver line separation	420m
Receiver line length	Up to 16,200m
Receiver arrays/line	100
Total number of dual sensor channels	800 per shot full spread
Prospect water depths	30 to 75m
Recording System	
Sample Rate (ms)	2ms
Record Length (ms)	6000ms
Tape Format	8058 SEG-D
Filters	Low Cut: 3 Hz, 6 dB/octave High Cut: 206, 275 dB/octave
Data channels	800
Geometry	
Acquisition Bin Size	15 x 30
Nominal Fold	40

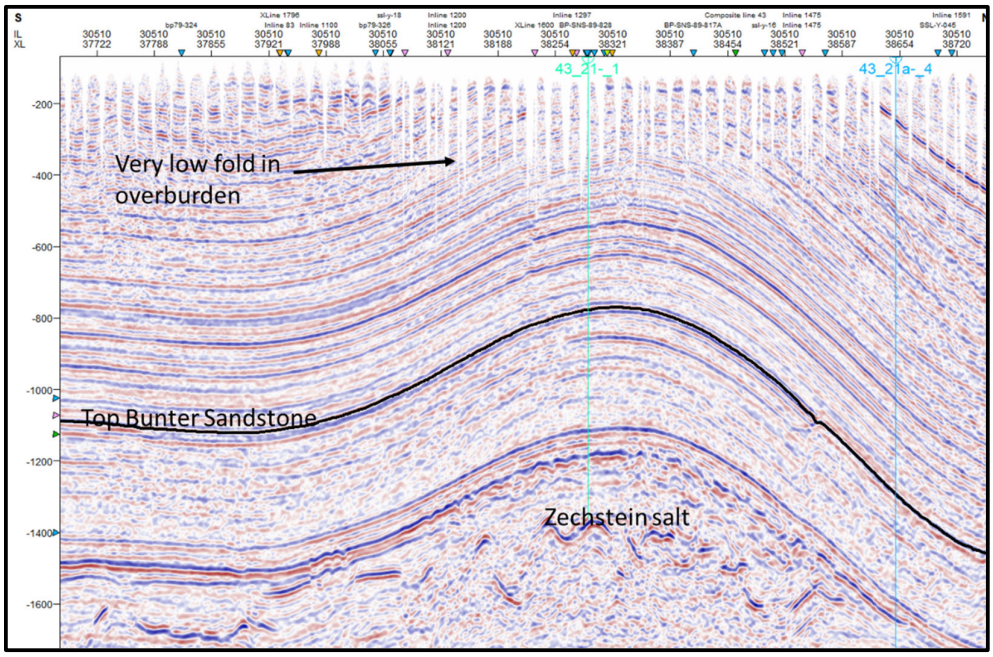

Figure 8 - Example of 1997 OBC 3D seismic data showing low fold in overburden and lack of general character through the section.

2.3 2013 Polarcus 3D Seismic

Subsets of the Greater and West Ravenspurn datasets were purchased for the project in mid-2019 to use for Endurance evaluation (red outline in **Figure 6**). The decision to purchase was based upon the coverage over the outcrop area, which was important to characterise for the project, and the overall higher fold and improved data quality.

2.3.1 Original Processing and Reprocessing Sequences

The original 2013 Polarcus data as purchased had some obvious deficiencies from being acquired and processed to only image the deeper pre-salt interval. The acquisition specifications are shown in **Table 3**. The gathers are not flat at the reservoir interval and were very harshly muted, limiting offset range and reducing fold at the Bunter Sandstone Formation level. There was also a lot of noise in the data that was considered as being relatively easy to remove (**Figure 9**).

Table 3 - Acquisition specifications for the 2013 Polarcus 3D seismic survey.

Survey	Polarcus Greater Ravenspurn MC
Acq. contractor	Polarcus
Field data format	SEGD
Tape format	3592
Vessel	M/V Nadia
Line prefix	MC1302-
Year of survey	2013
Sample rate (ms)	2
Record length (ms)	6200
Source	Dual
Source volume (cu/in)	4760
Source separation (m)	37.5
Source depth (m)	7
Gun delay (ms)	200
SP interval (m)	18.75 (flip/flop)
Cables	8 x 480 groups
Cable length (m)	6100
Cable depth (m)	12
Cable separation (m)	75
Near channels	1, 481, 961, 1441, 1921, 2401, 2881, 3361
Group interval (m)	12.5
Nominal fold	80
Nominal near offset (m)	100
Acquired bin size (XL x IL) (m)	6.25 x 18.75

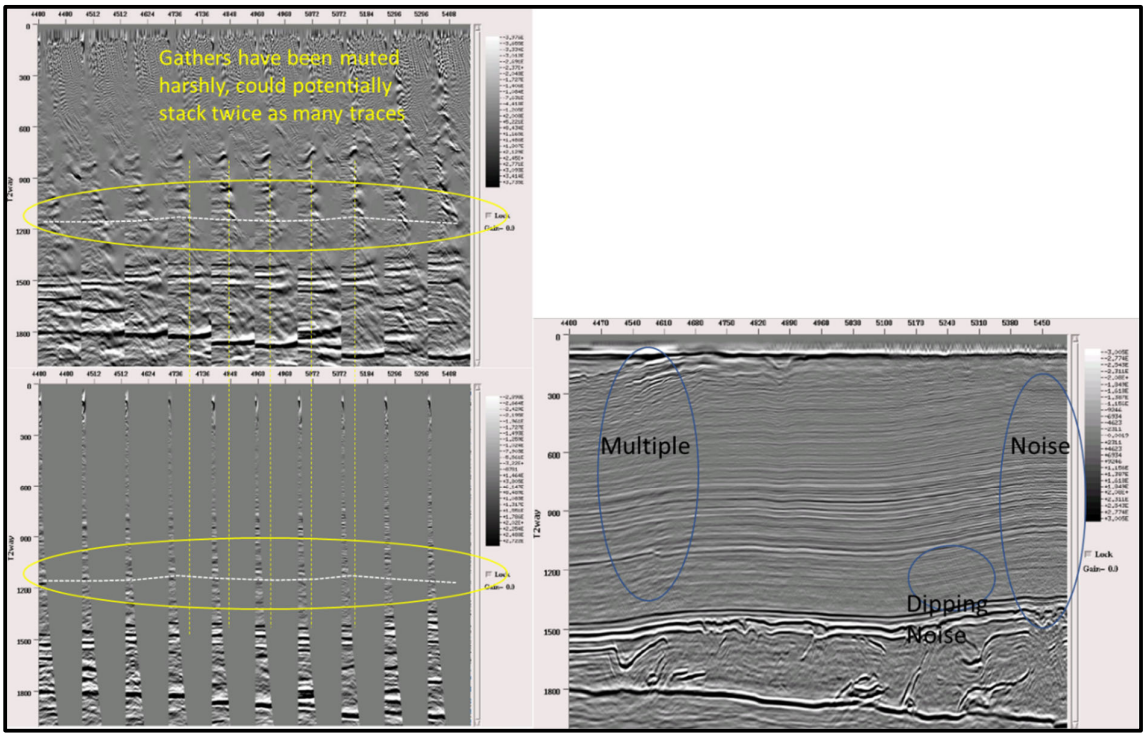

Figure 9 Reasons to reprocess the Polarcus 3D: harsh muting on the gathers has limited Bunter fold and many sources of noise could be removed.

The project decided to reprocess the data to improve the image quality at the Triassic level and reduce the noise, so a short post-migration reprocessing project was undertaken with CGG for 7 weeks. The original processing sequence for the data is shown in **Figure 10**. There was already significant processing applied to the data before the gather output after residual 'de-ghosting', which was the starting point for the new reprocessing. A summary of the CGG reprocessing workflow is shown in **Table 4**.

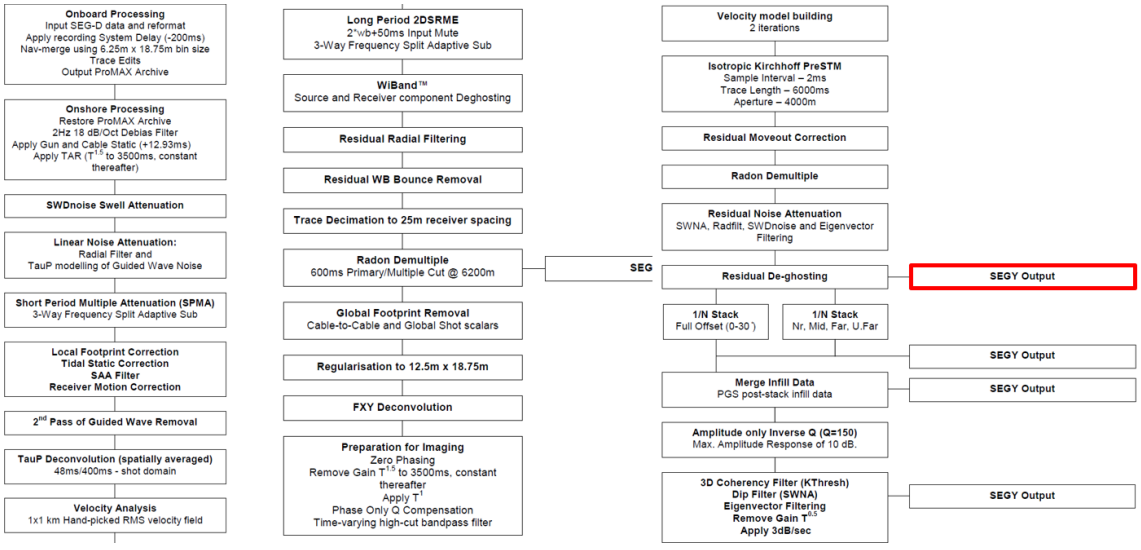

Figure 10 - Original Polarcus processing sequence for the data as purchased. Gathers after residual de-ghosting were available to reprocess.

Table 4 - CGG post-migration reprocessing sequence.

Reprocessing Sequence for Greater/West Ravenspurn 3D Data
Reverse polarity (increase in AI = positive peak) Anti-alias resample to 4ms. Anti-alias K-filter CDP domain
3D anti-leakage Fourier interpolation of Western volume onto Greater processing grid
Separate processing of Western and Greater Ravenspurn datasets
Residual Move-Out Correction
CDP De-Noise & De-Multiple: Matching pursuit linear noise removal: Transform -1000 to 1500ms Cut -60 to 60ms Reference offset 6060m 500ms AGC Low cut 3Hz Low pass 6Hz. Polynomial De-Noise: 11 polynomials Matching pursuit linear noise removal: Transform -1000 to 1500ms Cut -60 to 60ms Reference offset 6060m 500ms AGC Low cut 3Hz Low pass 6Hz. Matching pursuit parabolic multiple removal: Transform -2000 to 2000ms

Cut -50 to 50ms Reference offset 6060m 500ms AGC Low cut 3Hz Low pass 6Hz.
3D De-noise: Common offset low rank sparse inversion 21 x 21 traces x 250ms
Gather Flattening: Greater and Western data interleaved through overlap First pass 0-50 degrees Taylor moving window calculation with networked inversion for application Second pass cross-correlation time-shifts
Further 3D De-noise: Greater Volume only Parametric tau-px-py transform Coherency preservation (addback) Applied between 36 and 60 degrees
NMO De-stretch: 80Hz max frequency 5dB limit
Volume Creation: Full angle stack 0-36 degrees Sub angle stacks 12 degrees increments 0-12 Near 12-24 Middle 24-36 Far

36-48 Ultra-Far 2 Term least squares Shuey AVO 0-36 degrees with pre-flattening
Structurally conformable filtering: Wavelet scale application Weighted Kuwahara filter Variable filter length per octave (lower strength than wellie 1)
AVO Structurally conformable co-filtering (STAVO): Wavelet scale application Weighted Kuwahara filter Wellie 1 filter lengths
Whitening – Full stack only: Voice 3 to 28 Max boost 20dB

2.3.2 Results of Seismic Reprocessing

The result of the reprocessing is an uplift in data quality (see **Figure 11**) but there are some outstanding data quality problems that could not be fixed post-migration: shallow water multiple removal, 60Hz frequency notch, and acquisition footprint (**Figure 12** and **Figure 13**). The final Endurance seismic volume is a merge of the Western and Greater Ravenspurn surveys which have different acquisition directions (**Figure 14**). Overall, we see that the Greater Ravenspurn data (eastern side) appears to have lower quality than West Ravenspurn due to high frequency noise. As all the on-structure wells are in the West Ravenspurn volume the seismic calibration is skewed towards this side and it is possible that the phase is not exactly matched across the merged volume. The final volume was Rötated 120 degrees following well calibration from 43/21-1.

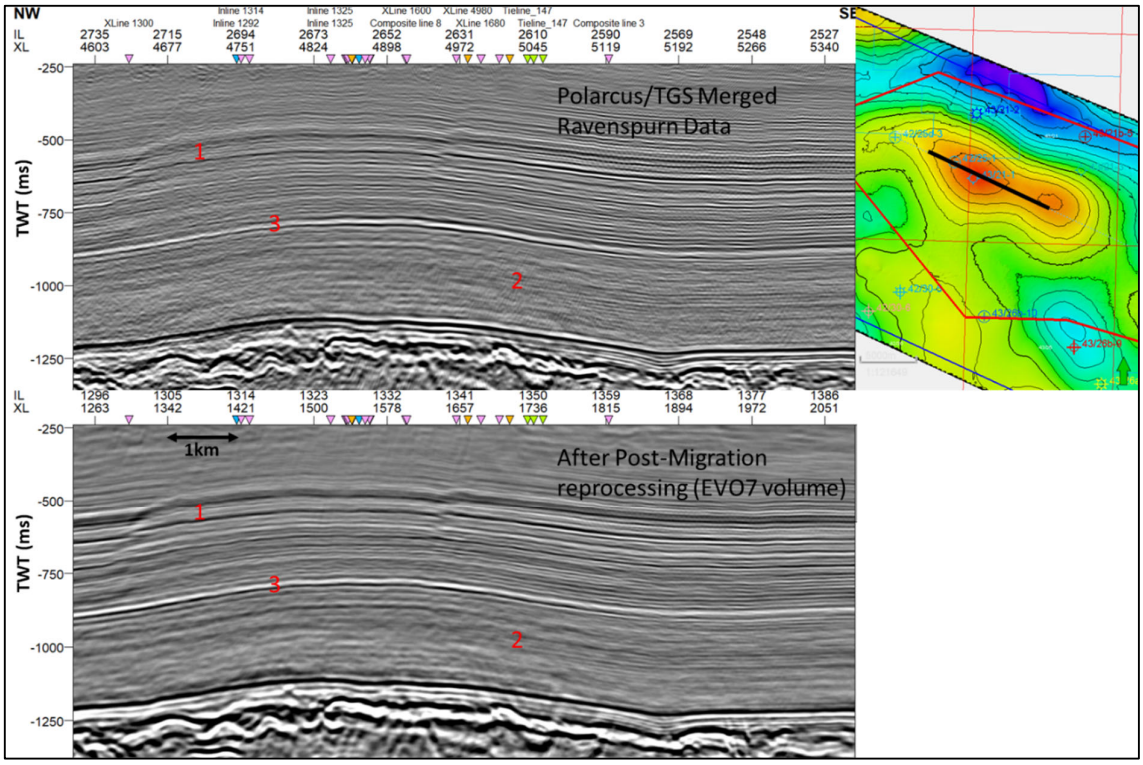

Figure 11 - Example of original Polarcus processing and data after post-migration processing. Some points to note: 1. Improved continuity in image; 2. removal of dipping noise; 3. better matching across West/Greater Ravenspurn surveys. Location of data shown in map inset (black line).

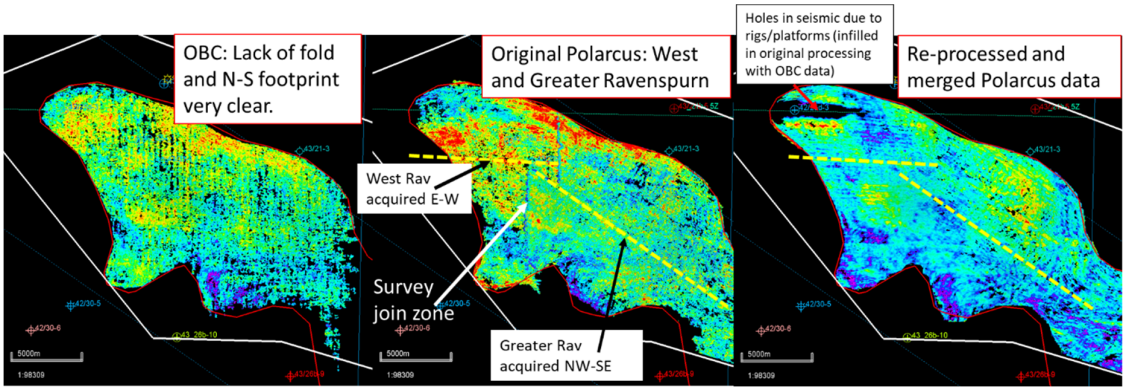

Figure 12 - Acquisition footprint at Top Bunter level demonstrated with horizon amplitude. The acquisition of the 2013 Polarcus 3D data in two surveys with different orientations means that there are two footprint trends in the merged volume. The N-S acquisition direction of the 1997 OBC data is also very clear.

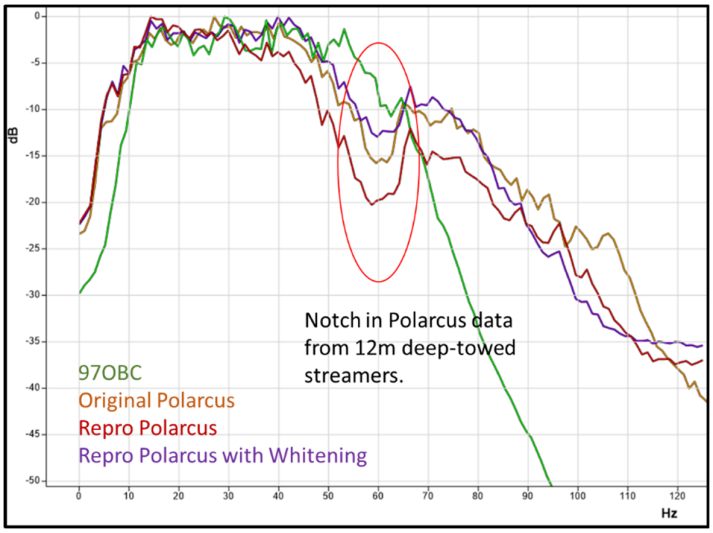

Figure 13 – Comparison of frequency spectra of the 3D seismic datasets. The 2013 Polarcus data has a notch at 60Hz but has more lower greater frequencies than the 1997 OBC data.

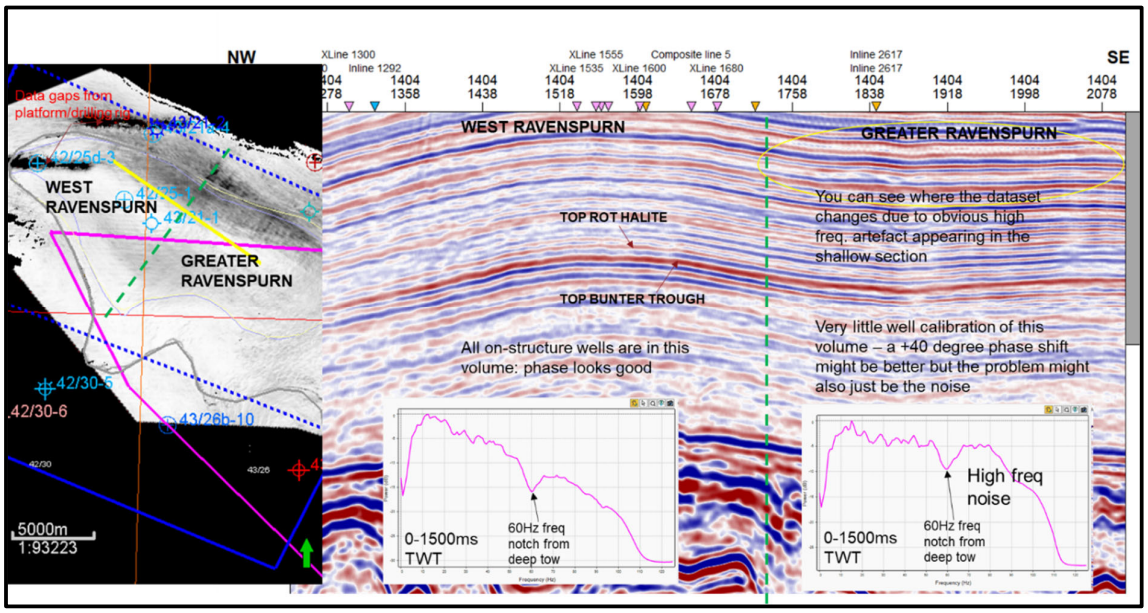

Figure 14 - Comparison of West and Greater Ravenspurn 2013 Polarcus datasets. The green dashed line indicates the boundary. Of note is the high frequency noise present in Greater Ravenspurn which appears to degrade image quality.

With these limitations in mind, and the observations from well ties and synthetics shown in the section below, no detailed seismic analysis or seismic reservoir characterisation can be undertaken on this data. Amplitudes do not represent rock properties and there is significant artefact remaining at reservoir level.

For further stages of the project it is recommended to either reprocess the 2013 Polarcus data from scratch and/or acquire new 3D seismic optimised for imaging a shallower section of the stratigraphy. The acquisition specifications of the 2013 Polarcus data mean that it will never be

the ideal product for imaging the Triassic section as the spread was very wide which results in the near offsets being around 450 m at surface. This translates to approximately 15° at Top Bunter Sandstone, meaning that the near offsets are not at all captured. The acquisition footprint of the data can be reduced but it is unlikely to be removed completely. The current recommendation is that a survey more akin to a 3DHR survey will provide the best Triassic coverage and this option will be worked as the project progresses to further stages.

3.0 Well Synthetics and Well-ties

The dataset available for well synthetics and well ties is mixed in quality and coverage. Synthetics were generated in an internal rock property toolkit for wells in the area of interest (AOI) which had sonic and density data. Some pseudo-density was also calculated and appears to be a good fit where the input data is of sufficient quality. A summary of the well data and seismic coverage is shown below (**Figure 15** and Table 5).

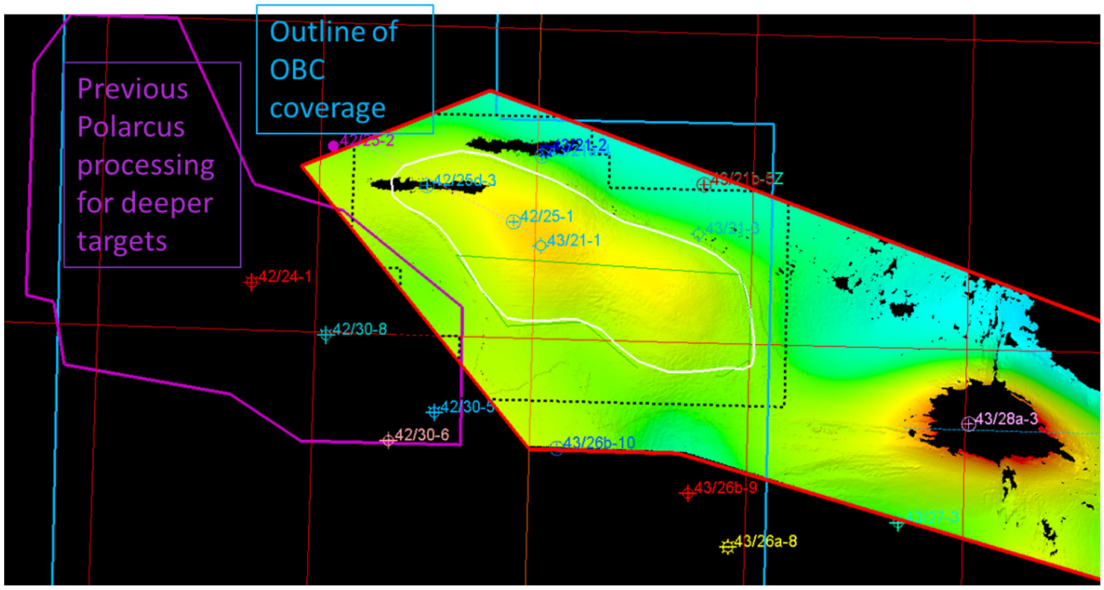

Figure 15 - Well locations across the different seismic volumes.

Table 5 - Summary of well/seismic coverage and sonic and density availability. Red = poor. Green = good. Yellow = some restrictions. Rptk: rock property tool kit.

Well	Best seismic volume	Sonic and Density log data
42-24-1	Original 2013 Polarcus	only sonic
42/30-5	Original 2013 Polarcus	no logs
42-30-8	Original 2013 Polarcus	only sonic
43/21-2	Garrow platform hole	only sonic
43/21-3	Reprocessed 2013 Polarcus	only sonic
43/26b-9	1997 OBC	only sonic
43/27-3	edge of 3D	only sonic
43/21b-5	Reprocessed 2013 Polarcus	only sonic
42/30-6	1997 OBC	from rptk
43/26a-8	1997 OBC	no
43/28a-3	top of outcrop – poor imaging	no
43/21-1	Reprocessed 2013 Polarcus	yes
42/25d-3	1997 OBC	yes
42/25-1	Reprocessed 2013 Polarcus	too short in reservoir
42/25-2	1997 OBC	yes
43/21a-4	Garrow platform hole	yes
43/26b-10	1997 OBC	yes

3.1 Well Synthetics

Well synthetics were created focussed on the Bunter Sandstone Formation reservoir and primary seal. The overlying primary seals are the Röt Clay and Röt Halite, which is subdivided into three sub-zones. The seismic response around the top of the Röt Halite 1 package (near top primary seal, at the top of the thick Halite section) is a trough (**Figure 16**). At the top of the Bunter Sandstone Formation, there is an unusual seismic feature, whereby a different seismic response is generated depending on where the well is located. Over the structural high and towards the outcrop the Bunter Sandstone Formation has high porosity and the response at the top of the formation is a trough. However, around the structure in a trend similar to, although not exactly coincident with the structural contours, the sandstone becomes cemented with halite, reducing porosity and making it acoustically hard, causing the seismic phase to flip to a peak (**Figure 17**). This is referred to as the Seismic Phase Reversal (SPR). The base of the reservoir is the top Bunter Shale Formation. This is a peak on all well synthetics (**Figure 18**).

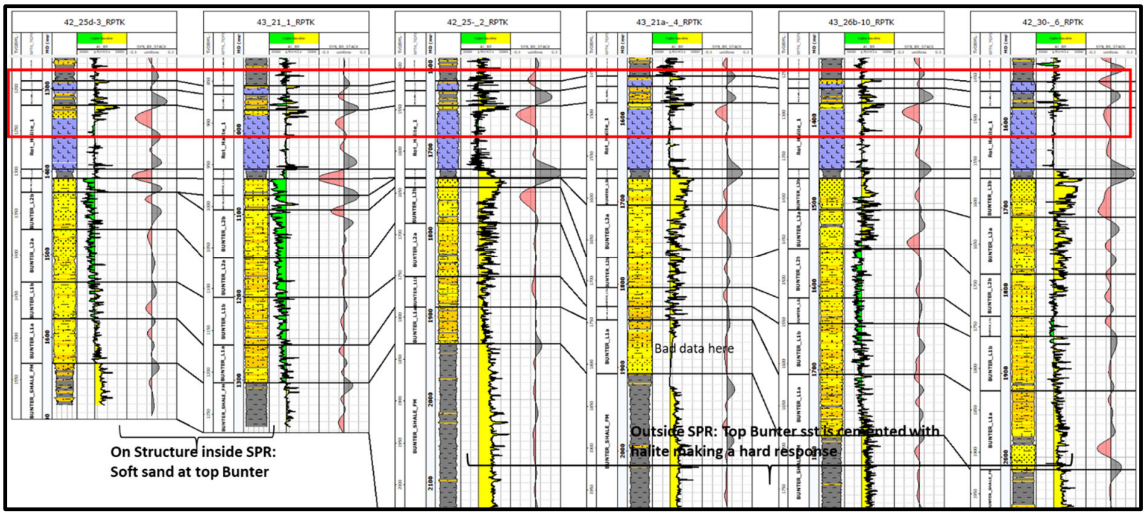

Figure 16 - Seismic response of the upper Röt Halite (outline in red box). All wells exhibit a consistent trough response.

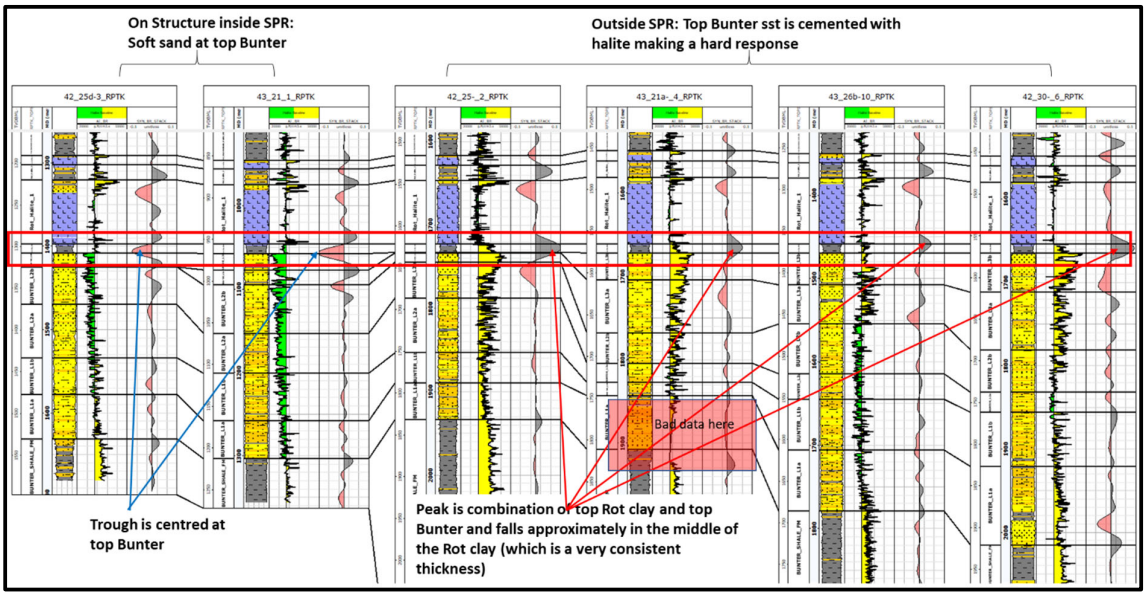

Figure 17 - Seismic response at Top Bunter Sandstone Formation (top reservoir). On structure where the sandstone is porous the seismic response is a trough but where the sandstone is cemented (outside the SPR) the response flips to a peak.

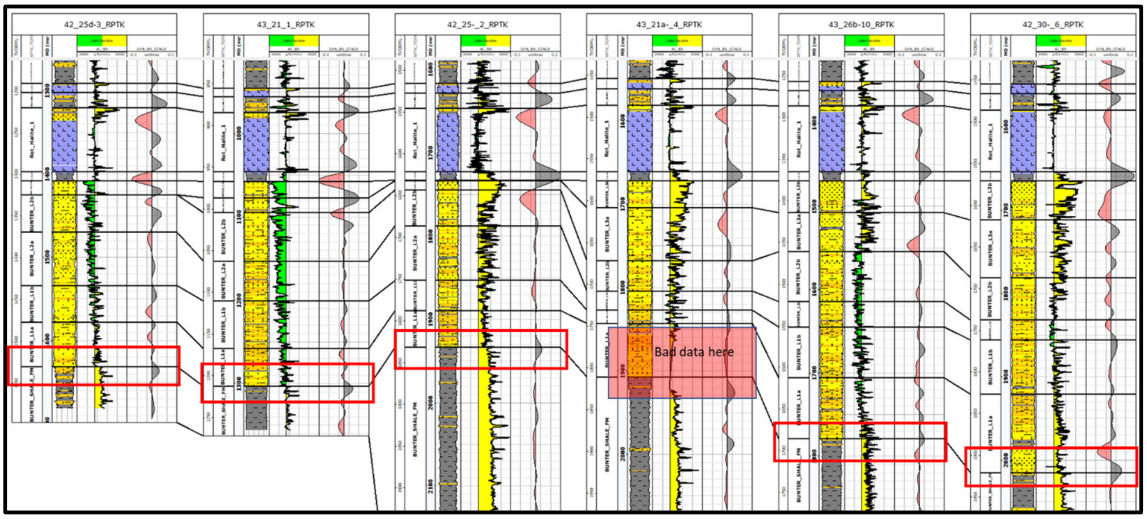

Figure 18 - Top Bunter Shale Formation (base reservoir) modelled seismic response. All wells predict a peak at the top of the shale.

3.2 Well-ties

The options for well-ties were limited given the lack of logs over the Bunter Sandstone Formation interval in many wells and the seismic/well overlap (Table 5). Two examples of well-tie are shown below (**Figure 19** and **Figure 20**). The only well which can be tied on structure, on the reprocessed 2013 seismic, is well 43/21-1 (**Figure 19**). The wavelet used was matched to the spectra of the seismic above the Zechstein salt. There is a reasonable match through the section but relative amplitudes don't appear to be reliable, especially the Top Bunter Shale Formation which is too weak on seismic. The off-structure tie of 42/25-2 shows the difference in quality between the reprocessed 2013 data and the 1997 OBC (**Figure 20**). Larger

amplitude events match well but lower amplitudes don't correlate. In comparison, the well-tie for 43/21-1 generally shows a good match on peak/trough events but poor amplitude fidelity, whilst 42/25-2 shows a generally poorer quality tie except for the larger amplitude events.

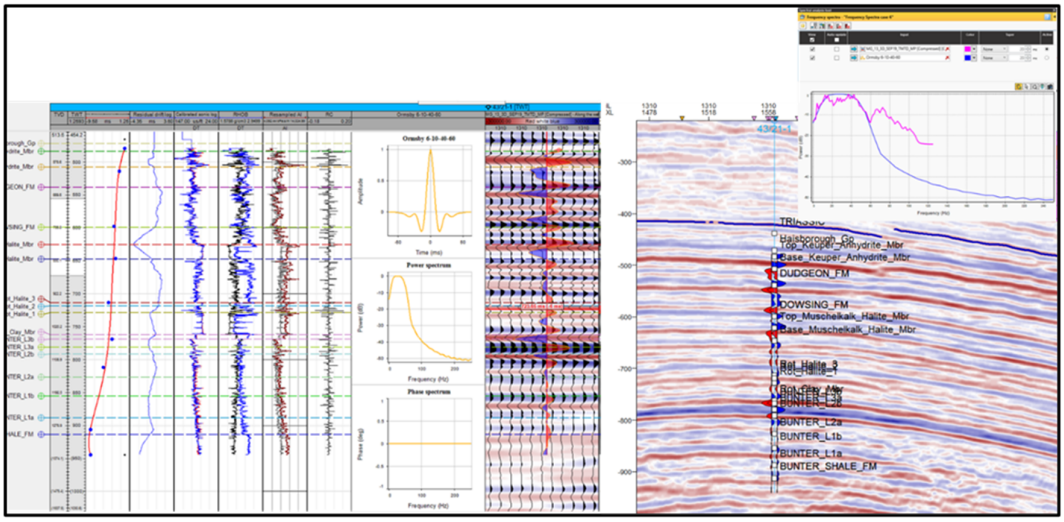

Figure 19 - 43/21-1 well-tie (crest of structure) on reprocessed 2013 Polarcus 3D seismic data.

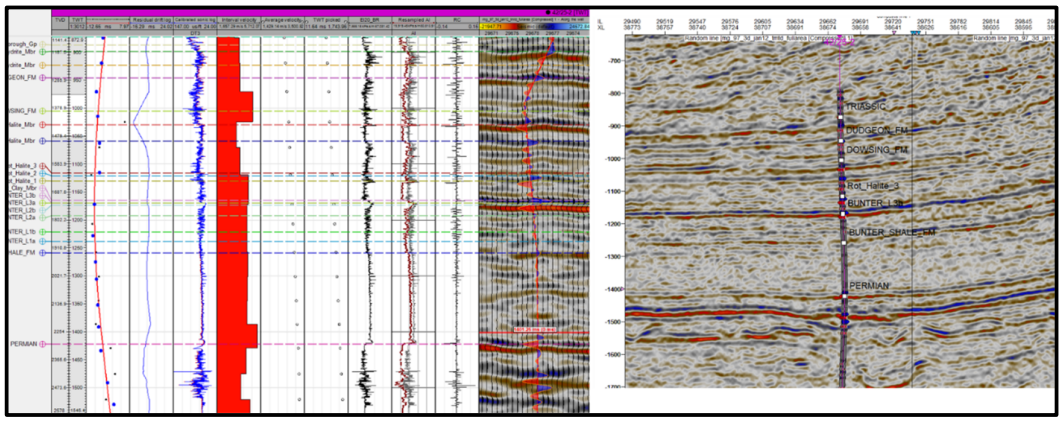

Figure 20 - 42/25-2 well-tie (downdip to west) on 1997 OBC 3D seismic data.

4.0 Horizon Interpretation

Eleven horizons were interpreted on the seismic data: Seabed, Base Quaternary, Base Cretaceous Unconformity (BCU), Top Chalk Group, Top Lias Group, Top Triassic, Top Röt Halite 1, Top Bunter Sandstone Formation, Top Bunter Shale Formation, Top Zechstein Group and Top Rötliegend Group. For the most part, the stratigraphy is clearly imaged on the seismic and is simple to interpret. The greater reflectivity of the overburden (shales, halites, anhydrites) allows their signal to be much greater than the background noise. Only minor fault offsets exist in the overburden and apart from those the response is consistent and thicknesses approximately isopachous. Therefore, seismic interpretation is not thought to be an area of uncertainty, except for the interpretation of the Top Bunter Shale Formation (which defines the base of the reservoir). The isopachous nature of the Triassic stratigraphy and the regional wells coverage mean that horizon interpretation is not a significant uncertainty.

4.1 Top Röt Halite 1 (seal)

The trough seismic response of the Röt Halite, around the top of the Röt Halite 1 package (the top of the thick halite section) can be mapped across the entire seismic volume (**Figure 21**).

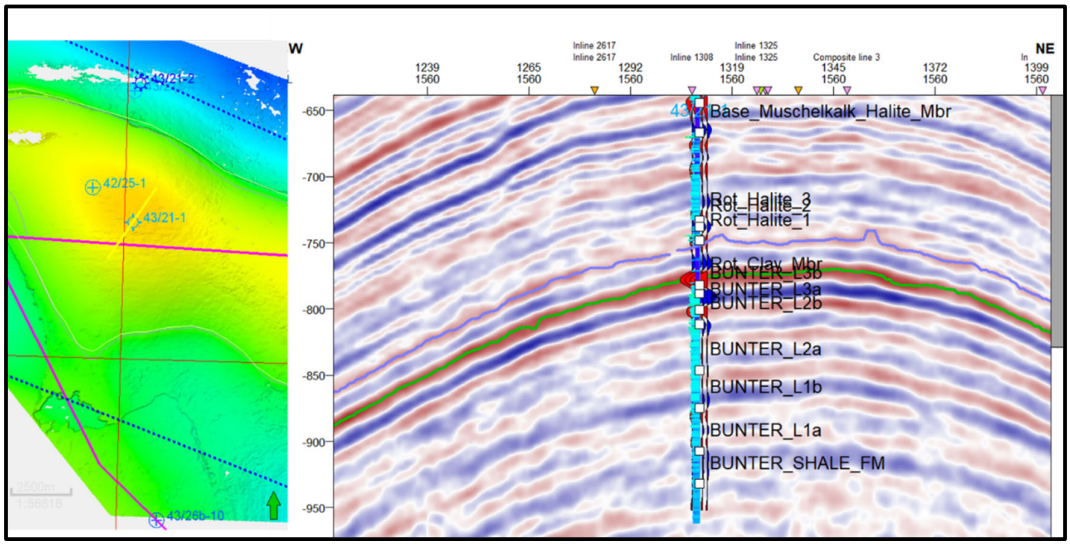

Figure 21 - Horizon interpretation of Röt Halite 1 over the Endurance structure (purple horizon) on a consistent trough.

4.2 Top Bunter Sandstone Formation (top reservoir)

As discussed above in section 0, the Top Bunter Sandstone Formation exhibits an unusual feature where the seismic response flips from a trough to a peak (Seismic Phase Reversal). The horizon interpretation was picked on a trough within the structural high and over towards the outcrop where the sandstone is high porosity, but beyond the SPR (which is similar to, though not exactly conformant to structure) it was picked on a peak. The SPR over Endurance is abrupt (**Figure 22**) and suggests a very sudden and complete flip to halite cementation in the upper reservoir downdip from this point. The salinity of the brine in the structure is very high and close to saturation (current brine salinity is 250,000 ppm, saturation point is circa

270,000 ppm) so it is believed that the precipitation of the halite was likely due to paleo-structure.

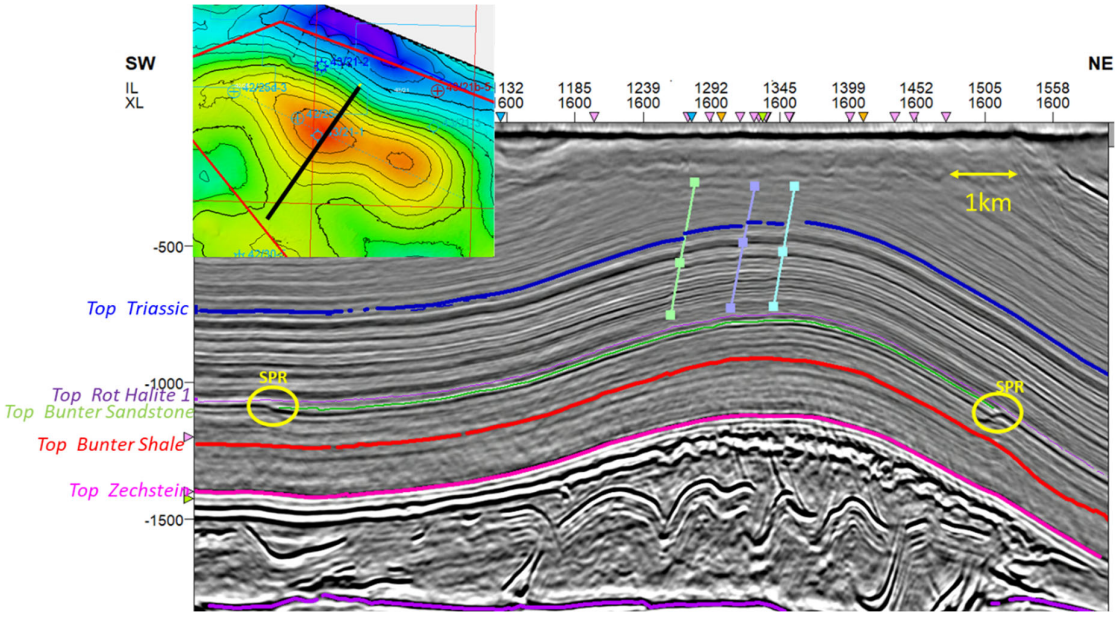

Figure 22 - Seismic Phase Reversal (SPR) observed in the Top Bunter Sandstone horizon interpretation, highlighted in yellow (section on 2013 Polarcus full-stack reprocessed seismic).

The Bunter sandstone is high net-to-gross and extensively reworked sandstone and there is very little predicted seismic character inside the reservoir. Acoustic Impedance (AI) contrasts below the uppermost section are small (**Figure 17**) and any units which are different tend to be very thin (~1m) and are not seismically resolved. Inside the SPR we see almost no reflectivity within the reservoir section; outside the SPR there is more variability due to the varying thicknesses of halite cementation. In well 42/25-2 the whole section is halite-cemented and there is no internal reservoir character. But in well 43/26b-10 the halite cementation stops at the base of the Bunter_L3a unit and there is strong trough as the sandstone porosity increases. In conclusion it is believed that the dominant reservoir character observed is the result of halite within the sandstone and doesn't indicate any other reservoir facies.

4.3 Top Bunter Shale Formation (base reservoir)

The Top Bunter Shale Formation was picked on a peak throughout the seismic dataset (**Figure 23**). This event does not tie particularly well on seismic: in the synthetics, the Top Bunter Shale Formation peak is modelled to be brighter than the reflectivity in the lower part of the overlying Bunter Sandstone Formation reservoir and should stand out, but in reality on the seismic data it doesn't and can only be interpreted in some areas based on continuity. This is likely the result of remaining noise in the seismic dataset impacting a relatively lower amplitude event.

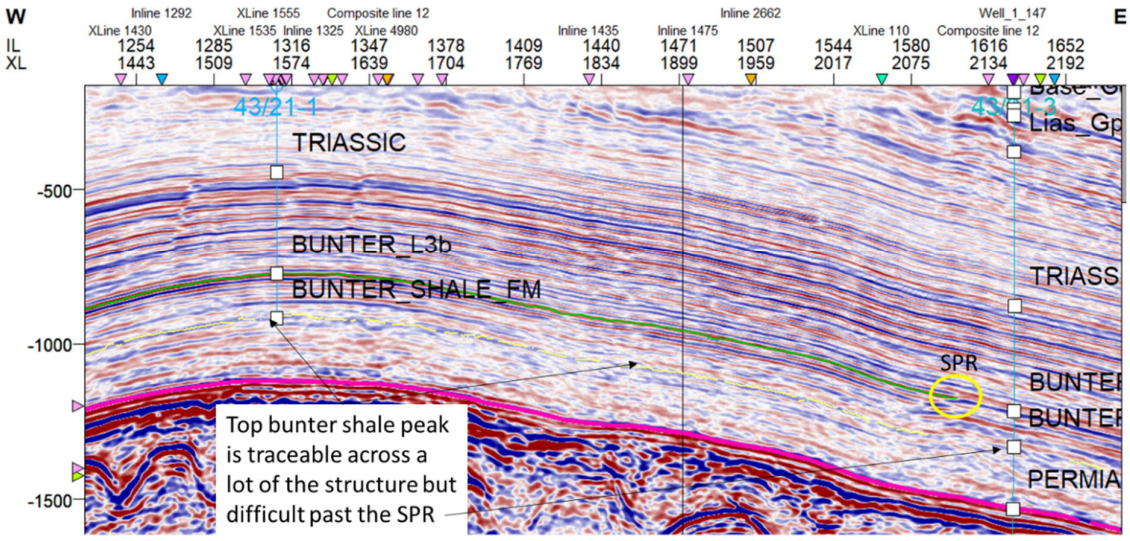

Figure 23 - Top Bunter Shale Formation (base reservoir) horizon interpretation (shown in yellow). The amplitude of this peak does not stand out against the background and in some areas the interpretation is low confidence.

5.0 Structural Evolution of the Endurance Salt Pillow and Diapir

The structural evolution of the Endurance structure is important to understanding the depositional history, along with the timing and nature of structures in the reservoir and seal. Timing of formation of the structure was one of the areas identified from gap analysis of previous studies. This was investigated here using sub-regional seismic interpretation and isopach analysis.

5.1 Growth of the Endurance Structure

The seabed at present day over the Endurance structure is a significant angular unconformity beneath a thin veneer of Pleistocene to recent sediments (**Figure 24**). Jurassic sediments currently subcrop the unconformity directly above Endurance crest. The effect of this unconformity is to remove all evidence of the growth history of the anticline which relates to any of the post Base Cretaceous Unconformity (BCU) compressional events which have affected the region.

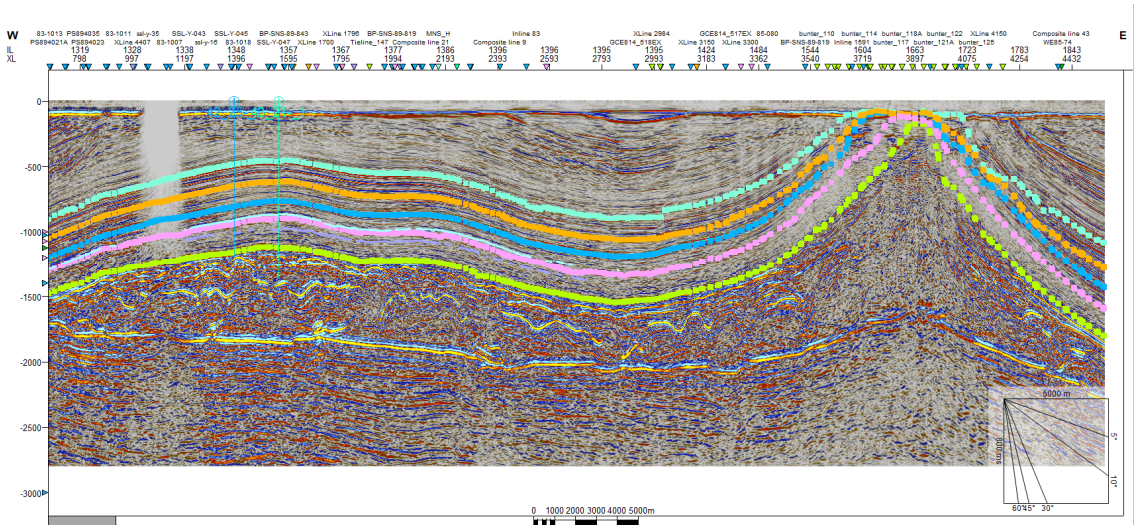

Figure 24 - Seismic section along the length of the Endurance structure and outcrop showing the unconformity at seabed, and apparent parallel nature of the top Bunter sandstone (blue), the top Zechstein (green) and Triassic reflectors (orange and pale blue).

Around the outcrop, above the Top Triassic, wedging reflectors indicate growth sometime after the BCU. Such reflectors cannot be seen over Endurance due to the unconformity. Reflectors within the Liassic section appear to be parallel to the top of the Zechstein salt, and no evidence of an angular unconformity exists within the Triassic or Liassic section, so it is concluded that the deformation postdates the shallowest Lias stratigraphy exposed at seabed. The outcrop to the southeast of Endurance shows evidence of wedging geometries postdating the BCU, which subcrops the seabed SE of the outcrop (**Figure 24**). This wedging constrains some movement of the outcrop, but since movement of diapirs in salt basins is strongly diachronous, this wedging does not provide direct evidence of movement of the Endurance structure itself.

The earliest the Endurance structure could have grown was the late Cretaceous, as this is the earliest significant tectonic event after the Liassic. This age is consistent with observation of wedging above the BCU on the outcrop. The structure may have been modified by later events, but there is no signal of this modification preserved. The unconformity at seabed could relate to any of the tectonic events during the late Cretaceous or early to mid-Cenozoic.

5.2 Structural Influence on Bunter Sandstone Formation deposition

If the deposition of the Bunter sandstone were influenced by pre-existing structure or halokinesis, facies or accommodation space may have been affected. Understanding any potential structural controls on Bunter sandstone deposition therefore has the potential to enhance understanding of reservoir heterogeneity.

The top Bunter sandstone reflector is well imaged on seismic and is close to parallel to the top Zechstein indicating little or no structurally controlled thickness variation in the entire Bunter package. The base of the Bunter sandstone is poorly imaged. As interpreted, there is a subtle thinning of the Bunter sandstone towards the northwest (**Figure 25**). There are no obvious

lineaments or changes in isochore gradient that could be attributed to underlying linear structural features. It can be concluded that there are no observable structural influences on Bunter sandstone deposition on the scale of the Endurance structure.

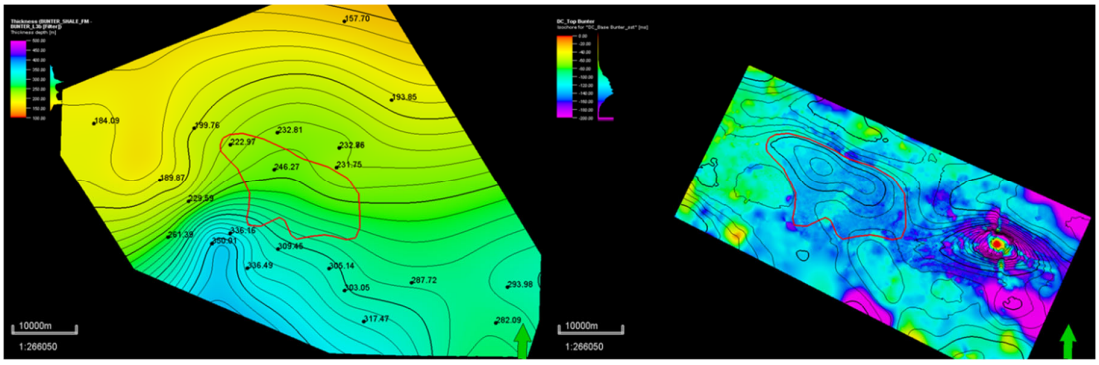

Figure 25 - Comparison of well thickness (left) and seismic time isochore (right) maps for the Bunter Sandstone Formation. Note the thinning to the NE on both images.

A thickness map for the bunter sandstone using well data from the area around Endurance (**Figure 26**) shows that it is strongly influenced by the large-scale geometry of the Sole Pit basin and the Dowsing fault zone. The thinning seen to the NW of Endurance is part of a broader trend that reflects the shape of the Sole Pit basin. While there is no observable field-scale control on Bunter thickness, regional controls do exist, with evidence for increased subsidence within the Sole Pit basin during the Triassic. This may be an effect of thinned lithosphere responding to regional subsidence, or local control by faulting. Faults controlling this subsidence are not observed and it is expected any faulting in the pre-salt stratigraphy to be strongly detached from the post salt stratigraphy.

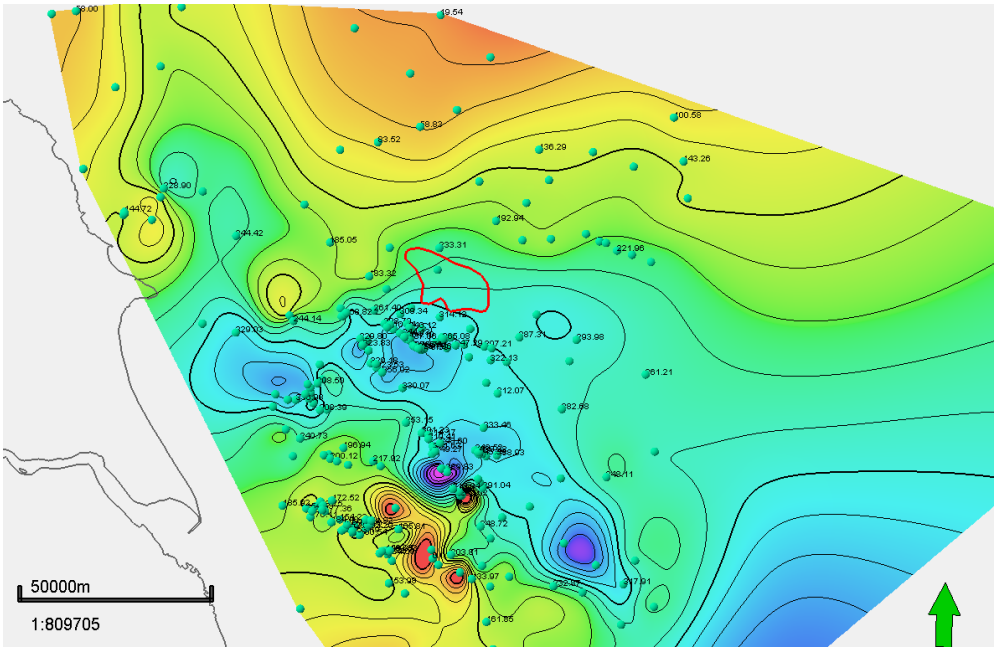

Figure 26 - Bunter Sandstone thickness isopach map from regional wells.

6.0 Fault Interpretation

Faults represent potential pathways for fluid leakage if the fault rocks are more permeable than the undeformed rocks, or if faults are prone to be dilatant, either as a result of regional stresses, or because of stress changes during injection into the reservoir below. Understanding the distribution of faults is therefore of key importance to the NZT/NEP project. Faults were mapped to understand both potential pathways through the seal, and as input into geo-mechanical modelling. Additionally, faults were mapped around the outcrop to try to understand the tectonic significance of such a structure, and to understand any potential lateral leak pathways away from the immediate overburden of Endurance

6.1 Overburden Fault Interpretation

Faulting is clearly imaged in the overburden above the Endurance structure (**Figure 27**). 98 faults were mapped on the reprocessed 2013 Polarcus seismic volume and Geoteric™ software was used to create seismic attributes to help QC the interpretation (**Figure 28**).

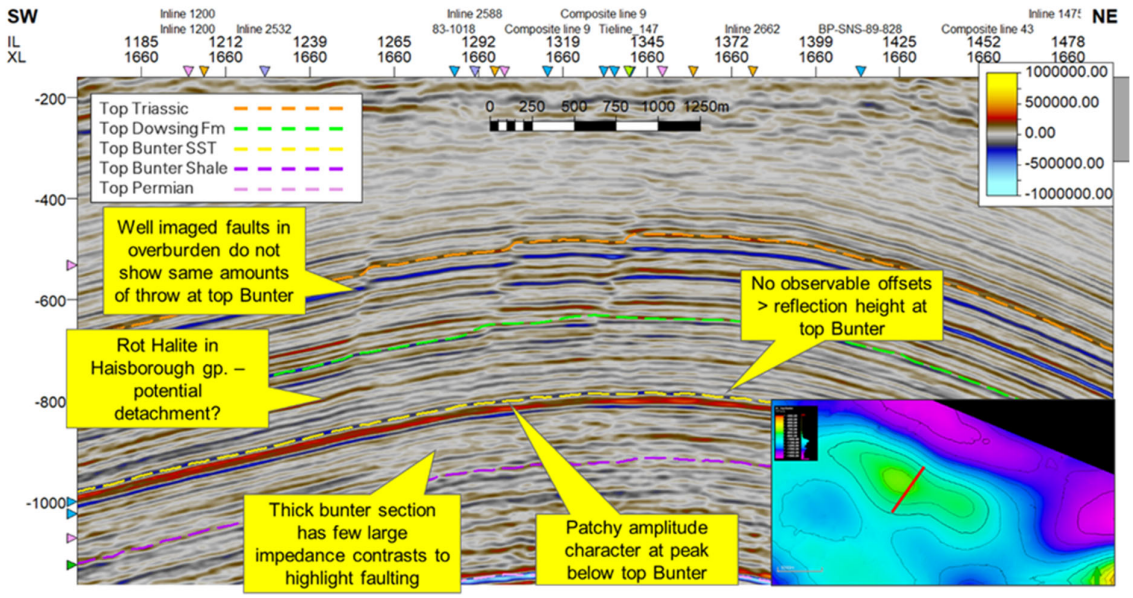

Figure 27 - TWT seismic section (reprocessed 2013 Polarcus data) showing faults in the immediate overburden above Endurance and the difficult seismic character in the reservoir section.

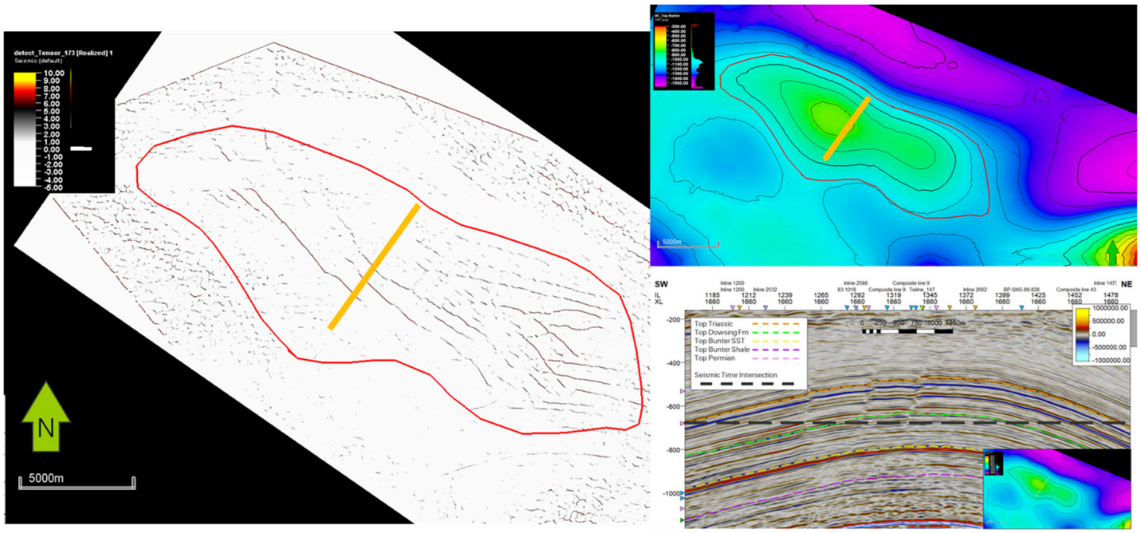

Figure 28 - Z Slice from Geoteric™ fault Detect Volume derived from the reprocessed 2013 Polarcus seismic volume and used to guide fault interpretation, showing overburden faulting over the Endurance structure but also acquisition noise (particularly clear around edges of volume). Reg polygon defines the approximate location of Endurance. Z Slice = 680 ms. Orange line if the location of section in Figure 27 and bottom right.

6.1.1 Fault Geometry

Faults over Endurance fall into 2 main trends – NW-SE trending faults, which occur over the crest of the Endurance anticline, and roughly E-W trending faults, which occur to the east of the Endurance structure and into the saddle between endurance and the outcrop (**Figure 29**). Complex cross-cutting relationships exist where the two trends intersect, resulting in a zone of short segments of both orientations of faults. The NW-SE trending faults dip dominantly to the SW, while the E-W trending faults dip to the N over the Endurance structure, and dip to both N and S in the saddle (**Figure 30**). Due to the resolution of the seismic volume at Bunter sandstone depths at the top of the anticline, we do not expect to be able to image faults with throws of less than 10-15m in the reservoir or overburden.

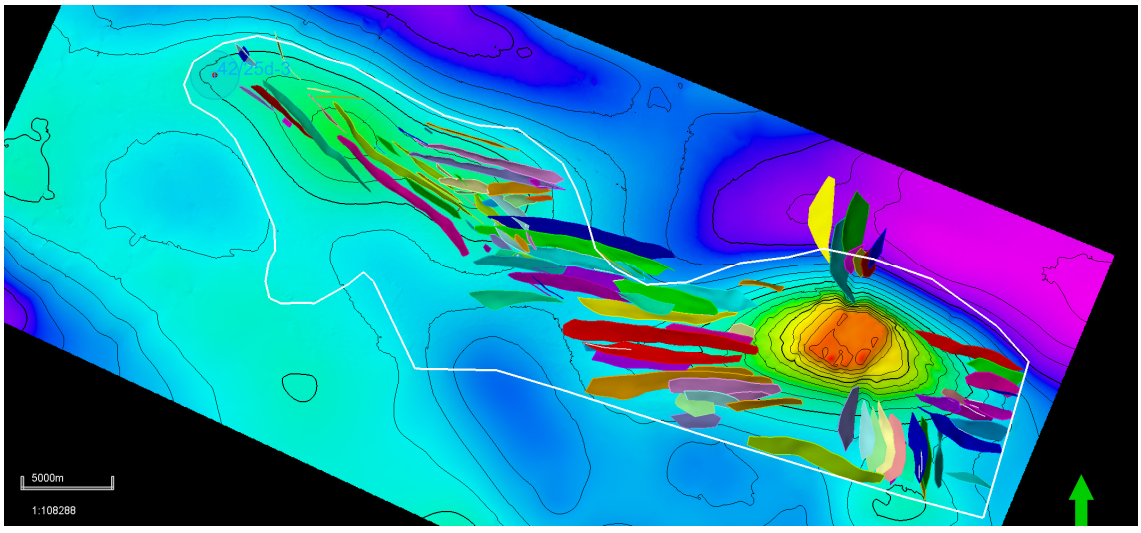

Figure 29 - Map showing 3D interpreted overburden faulting above Endurance and the outcrop. White polygon roughly defines the AOI for the interpretation, defined by the seismic phase reversal.

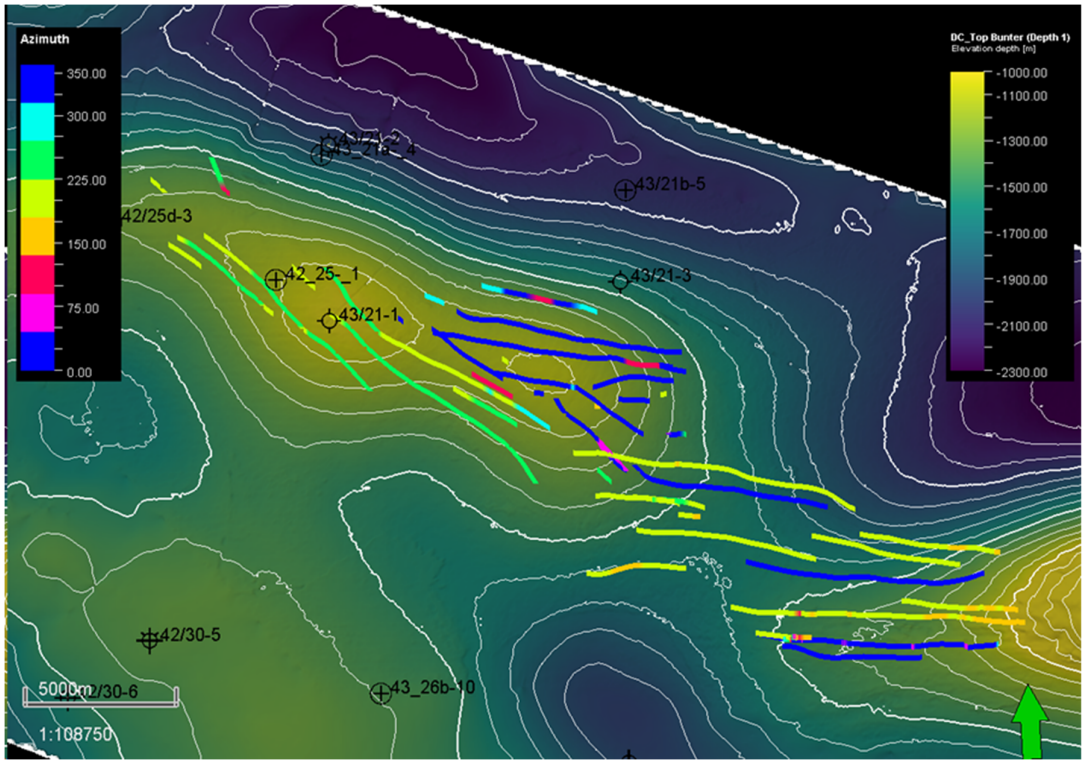

Figure 30 - Faults in the Endurance overburden coloured by dip direction, highlighting fault dip domains: NW-SE faults predominantly dipping to the N; E-W faults dipping both N and S.

Around the outcrop, the E-W trend of faults continues, and is present on the Eastern side of the outcrop in addition to the West. There is also an NNW-SSE trend of faults cutting across the outcrop. Extrapolating the two trends across the outcrop, the highest point of the outcrop is where the two trends would intersect (**Figure 29**).

6.1.2 Fault Offsets

Above Endurance, overburden faults can have significant offsets (throw > 30m at the top Triassic). Offsets appear to decrease downwards towards the Haisborough Group (**Figure 31** and **Figure 32**). Of the faults which intersect Röt Halite, the largest throw at the top of the Röt Halite is less than 15m, which is close to the resolution of the seismic data and may be an artefact of the fault polygon generation process. No faults can be observed deeper than the Röt Halite over the Endurance structure. Faults that cut the top of the Röt Halite are thought to detach within the halite and therefore are not expected to connect to the top Bunter sandstone (**Figure 33**).

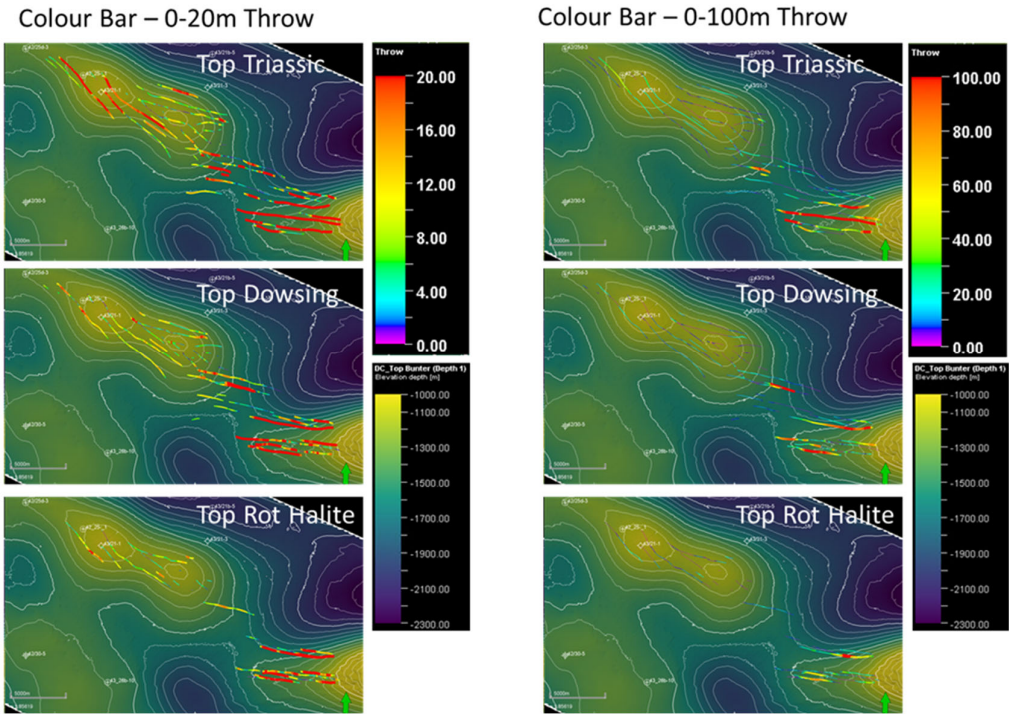

Figure 31 - Maps of fault throw for all mapped faults at 3 different horizons. Note throw decreasing towards the top Röt Halite.

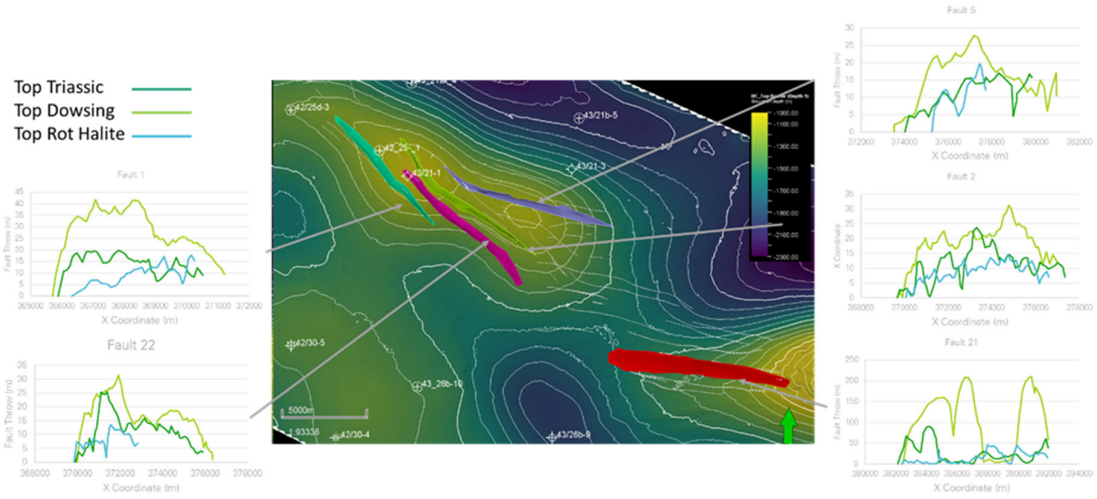

Figure 32 - Plots showing throw vs distance along fault for selected faults. Note the systematic reduction in throw towards the top Röt Halite. Based on the throw distribution, fault 21 is probably 2 separate faults, each with large throw at the top Triassic, and minimal throw at top Röt Halite.

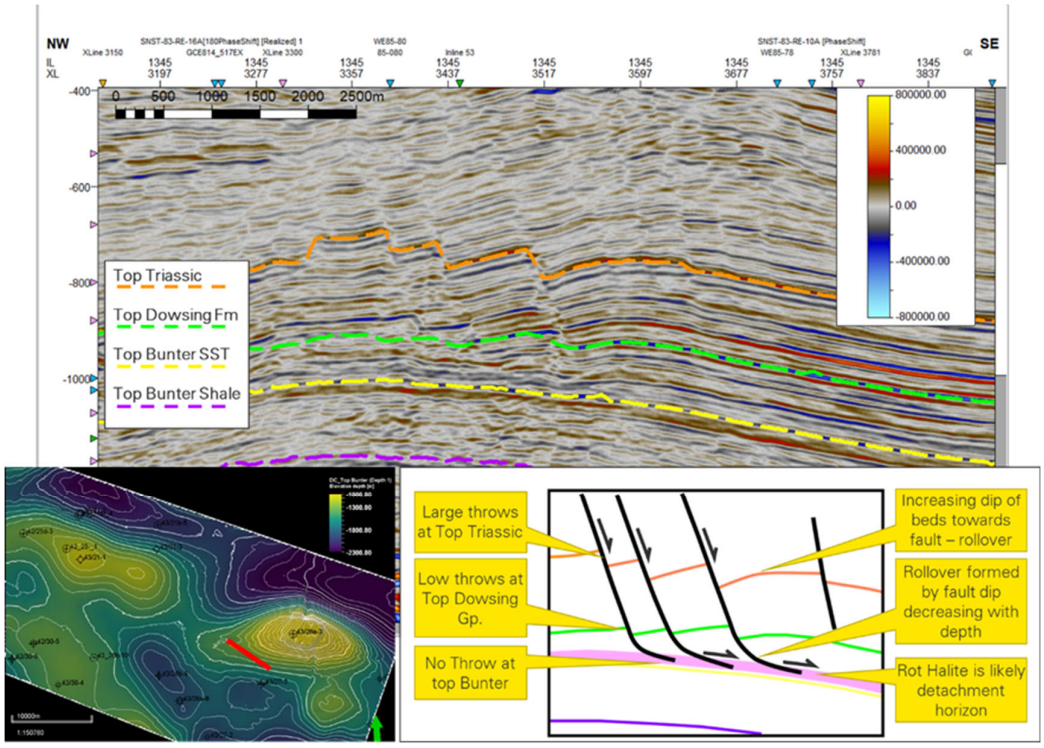

Figure 33 - Röt Halite acting as a detachment to the south of the outcrop top: Reprocessed 2013 Polarcus seismic line showing faults apparently detaching above Top Bunter. Bottom left: location map of seismic line (red line) relative to Endurance and the outcrop. Bottom right: simplified geological section showing the geometries seen on the seismic line.

At the outcrop, faults have much larger offsets than faults over the Endurance structure. (Figure 17, 18) Some faults show >150m throw at top Triassic. Locally, some faults cut the top Bunter sandstone, though other faults in the outcrop area are clearly detached on the Röt Halite, showing rollover geometries and lack of faulting at top Bunter beneath detached faults (**Figure 33**).

6.1.3 Fault Timing

The age of faulting in the Endurance overburden is uncertain, mainly due to the presence of the seabed unconformity which has truncated the faults. No evidence for growth stratigraphy can be seen, so the timing of the faults cannot be ascertained, other than being later than the Liassic, which is the youngest stratigraphy offset by the faults. Faults associated with the outcrop diapir cut the Base Cretaceous Unconformity (BCU), suggesting fault movement may have post-dated BCU, though these faults may have been localized around a diapir with a different history to the Endurance structure. There is no evidence that faults have been Rötated with bedding – faults have similar dips regardless of bedding dip, so it can be concluded the faults in the Endurance overburden postdate (or are contemporaneous with the late stages of) the folding.

6.1.4 Origin of Faulting

The simplest explanation for the faults in the overburden is that they are genetically related to the fold. Faults commonly form above anticlines in response to ‘outer arc extension’ – whereby the bending of relatively stiff beds is accommodated by tension on the outer arc of the fold and compression on the inner arc (Price and Cosgrove, 1990). The presence of ‘weak’ beds, such as shale or salt can lead to detachment between beds during folding, known as ‘flexural slip’ folding. Flexural slip folding can lead to different structural styles or geometries in the separate discrete brittle packages separated by those detachments.

The main challenge to this explanation is that the faults do not dip towards the centre of the structure in a typical crestal collapse geometry. Those ‘textbook’ geometries are not the only way these structures can form, as pre-existing structures and local stress variation can have a strong effect on fault geometry. The presence of detachments in the Röt halite (Stewart & Coward, 1995) likely has a strong influence on the development of faults, and a potential hypothesis for the evolution of the faults is that they relate to sliding on the detachments down dip, rather than to direct outer arc extension. A detailed understanding of the timing and geometry of the anticline would be useful in understanding the formation of the overburden faults and is unfortunately impossible due to the unconformity at seabed.

The intersection between the two fault trends at the outcrop could conceivably be the reason the outcrop is a much steeper, tighter structure than the Endurance anticline, if the long-lived structure influenced halokinesis locally. Such lineaments do not appear to be present beneath Endurance, which could explain the relative amplitude of the two structures.

6.1.5 Implications for Seal Integrity

Faults represent a potential leak pathway in the event they connect to reservoirs through sealing lithologies and have enhanced permeability relative to their surrounding rocks. Fault rock permeability could be enhanced by open fractures in the fault core or damage zone, or by the fault being critically stressed and dilatant.

6.1.6 Fault Permeability and Connection to the Bunter Sandstone Formation

The Liassic section above Endurance is predominately a mixture of fine-grained silts and mudstones, and any fault rock in the Liassic section is likely to be composed of similar and is not likely to be any more permeable than the host lithology (Ingram & Urai, 1999) unless critically stressed, open fractures are present. The same can be said for the upper Triassic section and Haisborough Group, which comprises a mixture of mudrocks and evaporites. Faults in such formations are unlikely to have permeable fault rocks due to the low permeability of the host formation. Open fractures could exist within damage zones around the faults, dependent on the lithification state of the rocks when they were faulted (Ingram & Urai, 1999). If rocks were brittle during deformation, it is conceivable open fractures may have formed, and if those fracture remained open and connected, faults may represent permeable pathways to the shallow subsurface or seabed. In Evaporite packages, such as the Muschelkalk or Röt Halite, it is not anticipated for any fractures parallel to faults, as the ductile rheology of these formations makes the presence of open, continuous fractures highly improbable.

Evaporites in the Haisborough Group (i.e. the Muschelkalk or Röt Halite) act as a detachment close to the outcrop (**Figure 33**), and this behaviour is documented elsewhere in the basin (Stewart & Coward, 1995). Over the Endurance structure, throws of faults progressively decrease towards the Röt Halite, and no evidence of faulting can be seen at the top Bunter Sandstone Formation, where there are no offsets on the Top Bunter Sandstone Formation horizon interpretation. The base case model is that the Röt Halite in the Haisborough Group acts as a detachment over the top Bunter Sandstone Formation. If the Röt Halite does detach deformation, it is assumed faults below the Röt Halite (i.e. faults in the Bunter Sandstone Formation) are not connected to the faults above the Röt halite (i.e. the clearly imaged overburden faults).

If overburden faults have a large enough offset, they may juxtapose the sealing Röt Halite against non-sealing lithologies and present a permeability pathway to shallower stratigraphy. Given the Röt Halite is approximately 100m thick over the Endurance structure, and the maximum recorded throw at the top of the Röt Halite is around 10-15m, this does not represent a likely outcome.

6.2 Reservoir Fault Interpretation

As discussed above, no faults can be seen deeper than the Röt Halite, in the Bunter Sandstone Formation or the Bunter Shale Formation, on seismic data (**Figure 27**). There are no observable offsets at top or base Bunter Sandstone Formation, nor are there any obvious or corelateable offsets of reflectors within the Bunter Sandstone Formation section. The Top Bunter Sandstone to Top Bunter Shale isopach is relatively constant and shows no linear features consistent with faulting, and the Top Bunter Sandstone Formation is also smooth, with no linear features consistent with fault offsets, in contrast to the upper Triassic section (**Figure 34**). The Bunter Sandstone Formation in well logs is acoustically homogenous, so strong reflectors within the sandstone may not be expected, further hampering our ability to detect faults.

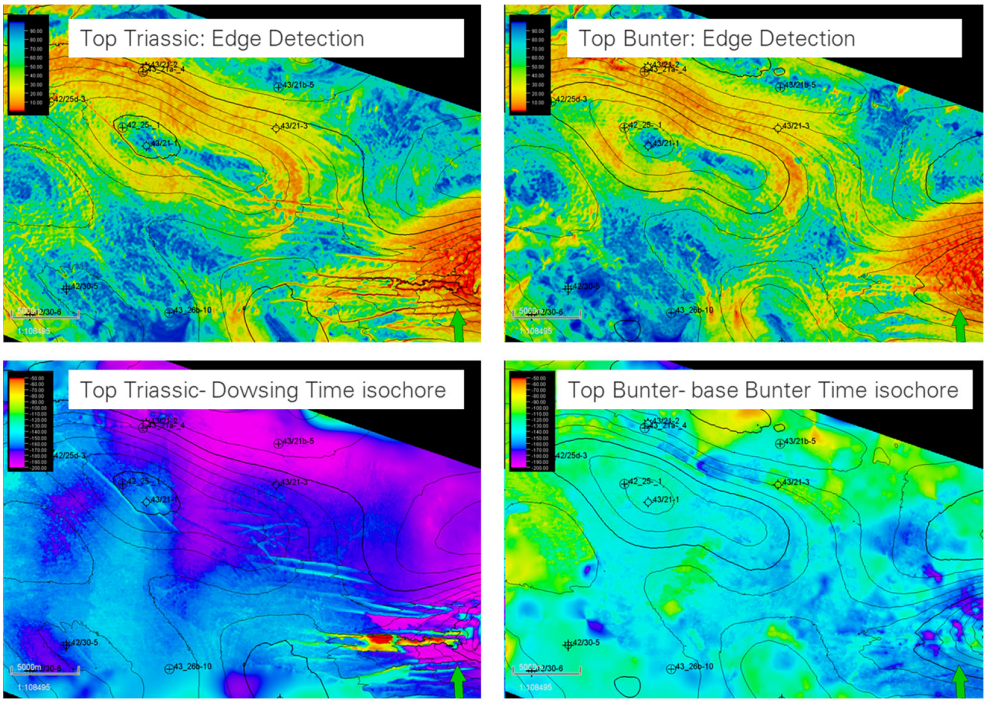

Figure 34 - Left: Top Triassic edge detection and Top Triassic-Top Dowsing time isochore showing clear lineaments associated with faults at the top surface. Right: Top Bunter edge detection and Top-Base Bunter time isochore. No Fault lineaments can be seen.

The Bunter has been deformed (folded) since its deposition, so it can't be ruled out that there is some faulting in the reservoir. Hints of deformation in the Bunter can be seen, but not correlated across multiple lines (**Figure 34**). Since no offsets of the top Bunter can be seen on seismic, it is inferred that any faults have throws small enough that they cannot be imaged seismically – likely <10-15m. If they represent significant baffles or barriers, such faults could still have a significant effect on reservoir injectivity; causing inefficient sweep of the reservoir, separating injectors from producers, and causing inconsistent pressure distribution across the reservoir.

6.2.1 Fault Mapping in the Bunter Sandstone Formation

Given the lack of imagery, faults could not be picked from seismic data. A series of fault detection attributes were attempted using Geoteric (Tensor, SOS, Dip), along with an amplitude extraction from an intra-Bunter pick (which may be a multiple) to visualize faults (**Figure 35** and **Figure 36**) but were unable to map consistent faults across multiple attributes. Instead, lineaments were picked on each of those attribute extractions. These were ranked by confidence for each attribute, then compared the lineaments from each attribute. Where multiple lineaments coincided, it was interpreted to be a 'master lineament', and the confidence attributes from the individual attribute lineaments were used to assign confidence to the master lineaments. Faults at Top Bunter Sandstone Formation are relatively well imaged around the outcrop and have higher confidence than those across Endurance (**Figure 35**).

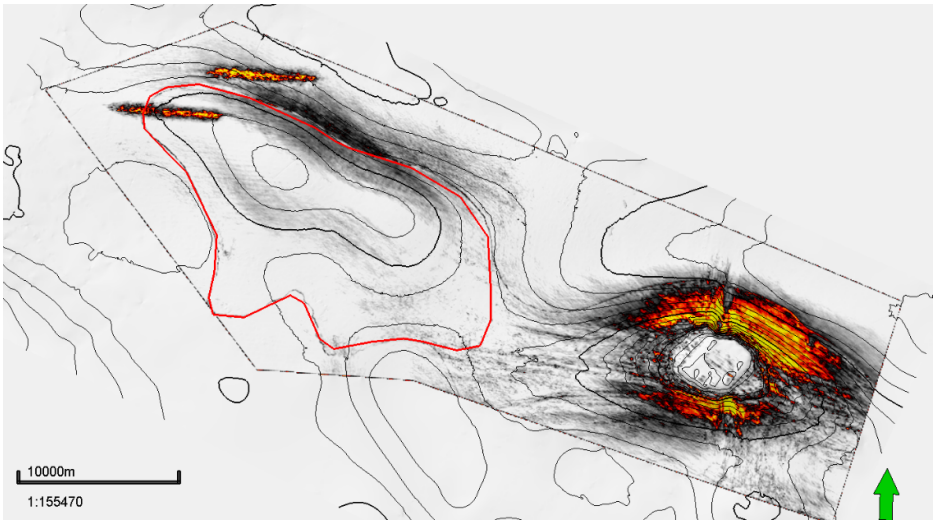

Figure 35- Variance extraction at the Top Bunter Sandstone Formation, showing the well imaged variance lineaments at the outcrop, compared with only faint lineaments over Endurance.

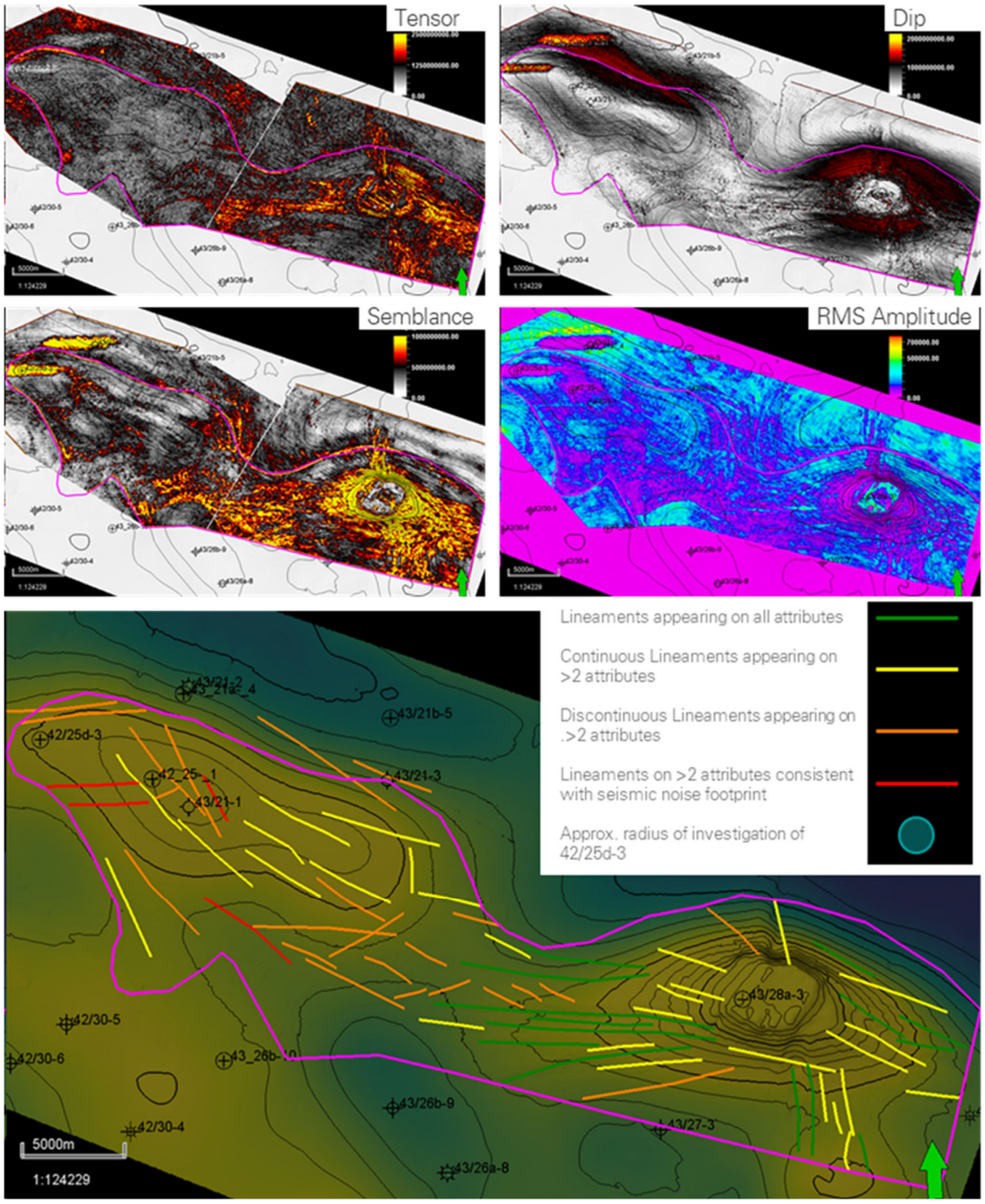

Figure 36 - The use of multiple attributes to generate a lineament map for the Top Bunter Sandstone Formation, coloured by confidence. The strong E-W lineaments to the NW of the survey are noise in the seismic volume, formed by gaps in the acquisition as a result of the vessel being unable to sail close to infrastructure

The master lineament set comprises lineaments in several orientations, but predominantly trending NW-SE (**Figure 36**). This is parallel to the trend of faulting in the overburden, but also to the acquisition footprint of the seismic data, which cannot be ruled out as the cause for some of these lineaments. Around the outcrop, lineaments form sets parallel to the overburden faults, which is expected as faults around the outcrop cut the top of the Bunter Sandstone Formation in several places.

Since any faults in the Bunter sandstone would be expected to have throws below seismic resolution (i.e. 10-15m), the several km lengths of the lineaments picked are unrealistically high. These faults therefore represent a pessimistic case in terms of fault lengths, and gaps in fault systems may enhance connectivity. No evidence of vertical barriers or baffles was interpreted from the 42-25d-3 well test, which extended to a radius of approximately 1.2 km (White Rose, 2016). The lack of vertical barriers in this test is evidence against pervasive baffling by closely spaced faults in the reservoir.

7.0 Velocity Model and Depth Conversion

A new velocity model was required to depth convert the reprocessed 2013 Polarcus seismic, as this has a different AOI to the previous White Rose (2016) velocity model. Unfortunately, the seismic velocities were not adequate to use in the velocity model build because where the two seismic surveys (West and Greater Ravenspurn) join the velocities did not match. The 2019 reprocessing was only post-migration (section 0) so a new velocity cube could not be generated. This would be an important output of any full reprocessing or new seismic acquisition. Given these restrictions a V0k model (layer-cake model with velocity gradients) was built that incorporated laterally varying velocities within the reservoir. Surfaces were flexed to wells to enable exact matching for input into the model, however, there are remaining uncertainties due to the lack of shallow overburden data and the spatial coverage of wells to calibrate to model.

7.1 Methodology

The model AOI extended outside of the seismic coverage, so well data was used more extensively in these areas (**Figure 37**). A summary of the well data available at the time of velocity model build is shown in **Table 6**. Other data may be available and could be used to update the model in future.

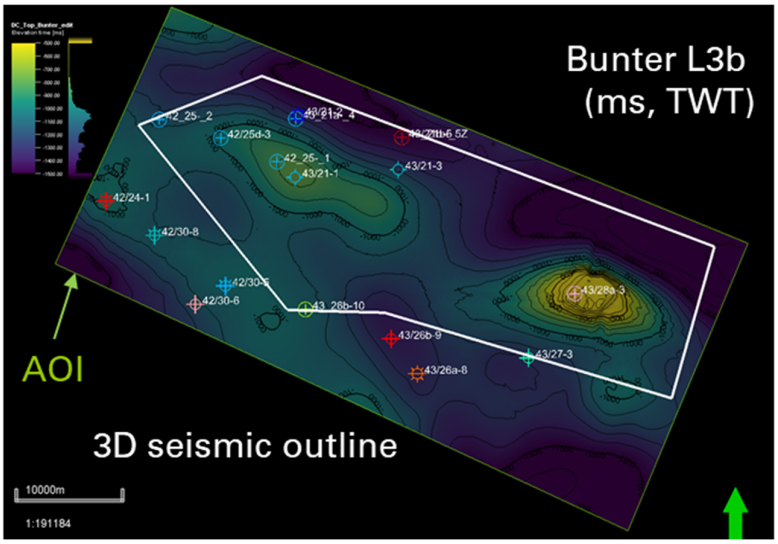

Figure 37 - AOI for velocity model and wells used in velocity model build.

Table 6 - Summary of available well data for velocity model build.

Area	Well Name	Checkshot	Sonic Log
Outside of 3D seismic	42/24-1	Yes	Yes
	42/30-8	Yes	Yes
	42/30-5	Yes	Yes
	42/30-6	Yes	Yes
	43/26b-9	Yes	Yes
	43/26a-8	Yes	Yes
On edge of 3D seismic	42/25-2	No	Yes
	42/26b-10	No	Yes
	43/27-3	Yes	No
Within 3D seismic	42/25d-3	No	Yes
	42/21-2	Yes	Yes
	43/21a-4	No	Yes
	42/25-1	No	Yes
	43/21-1	No	Yes
	43/21-3	Yes	Yes
	43/21b-5	No	No
	43/21b-5Z	No	Yes
	43/28a-3	Yes	Yes

The primary source of data for the first stage of velocity model build were the checkshots. These were QC'd to remove any anomalous points and define the initial V0k trends. These were then compared to the sonic log data and the trends updated, which was iterated through a number of times to create a basic model which honoured the data. The final V0k parameters are shown **Table 7**.

Table 7 - V0k parameters for background velocity model.

Layer	Top Surface	Base Surface	V0 (m/s)	k
0 – water	n/a	Seabed	1480	0
1	Seabed	Top Triassic	1900	0.811
2	Top Triassic	Top Bunter Sandstone	2300	0.702
3 – reservoir	Top Bunter Sandstone	Top Bunter Shale	(variable)	(variable)
4	Top Bunter Shale	Top Zechstein	3000	0.6602
5	Top Zechstein	-3000 ms	3100	0.6056

There is a trend in the Bunter Sandstone Formation velocity which is created by the halite cementation. On the western side of the model the sandstone becomes strongly cemented with halite all through the reservoir off structure (section 0). On two-way time (TWT) seismic data this appears as a thinning of the sandstone but it is actually a velocity effect (combined with a slight thinning) because the halite increases the velocity by around 20%. In order to correctly depth convert top and base reservoir for the model this factor needed to be incorporated. A seismic-derived surface was required to add in this change spatially because the well coverage is not dense enough. As the velocity change causes a decrease in TWT, the Top Bunter Sandstone – Top Zechstein isochore was used as a proxy for reservoir velocity in this area (Top Bunter Shale interpretation was not suitable due to uncertainty of horizon interpretation). The isochore was calibrated to sonic logs and a laterally varying cube of this velocity was generated (**Figure 38**) and used to replace the existing V0k reservoir layer in the model.

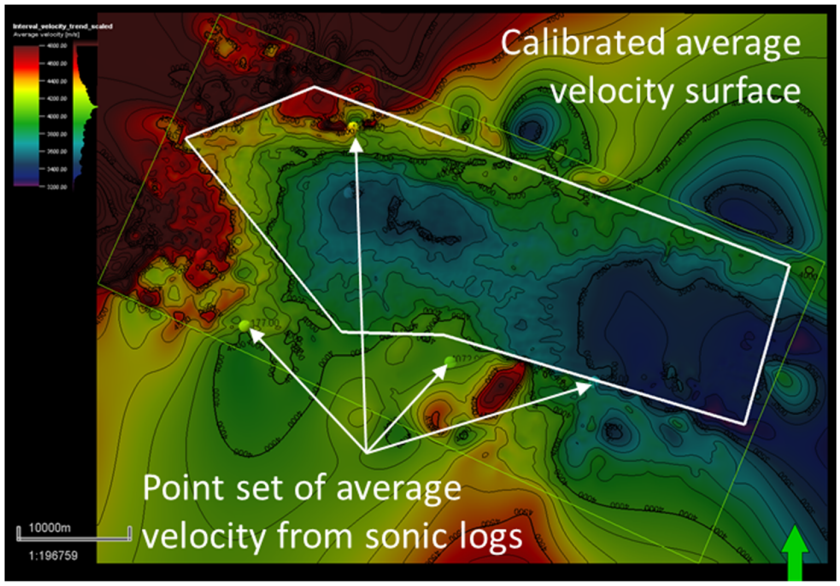

Figure 38 - Laterally varying reservoir velocity layer (layer 3).

7.2 Velocity Model Calibration

The velocity model calibration used a subset of wells where there were coincident log data, seismic coverage and confident interpretation, and well picks (to ensure that the seismic interpretation and tie to the well pick was correct). This excluded the Seabed and Top Bunter Shale from all calibration and was quite sparse in general (**Table 8**). Following this there were clear mis-ties for many of the surfaces and these were flexed to fit using an 8 km radius. The result of the flexing varied the structure but did not vary the reservoir thickness which suggests that the velocity errors are likely to be in the shallow overburden where the data is particularly poor. For the wells with seismic coverage the Top Bunter Sandstone mis-ties were small (1.3 – 5.5 m). The mis-ties of wells outside of the 3D seismic area were much higher (Table 9) which is due to interpolation of 2D interpretation, and is likely also to be impacted by the changing overburden as we move off structure with the chalk unit being present in the shallow section which is not covered by sonic data in any wells in the AOI. When the mis-ties are shown in map view (Figure 29) a clear west–east trend is observed. The iteration of the V0k overburden has produced a good average trend for the whole AOI but it appears that there must be a strong lateral trend in overburden velocities that will need to be investigated further with future data updates.

Table 8 - Velocity model calibration summary.

Well Top	42/25-1	43/21-1	43/21-3	43/21b-5
Seabed	N	N	N	N
Top Triassic	Y	N	Y	Y
Top Bunter Sandstone	Y	Y	Y	Y
Top Bunter Shale	N	Y	N	N
Top Zechstein	N	N	Y	Y

Table 9- Final mis-ties pre and post-flexing for all wells in AOI.

Well	Include in calibration	Comments	Mis-tie pre-flex	Mis-tie post-flex
42/25-1	Y	Seismic pick updated	33.82	0.0
42/25-2	N	Edge of 3D	-86.95	0.0
42/24-1	N	Far outside 3D area	-284.21	0.0
42/25d-3	N	Gap in seismic data – do not use	-107.81	0.0
42/30-5	N	Far outside 3D area	-79.88	0.0
42/30-6	N	Far outside 3D area	-85.75	0.0
42/30-8	N	Far outside 3D area	-208.88	0.0
43/21b-5z	N	Deviated; discrepancy with 43/21b-5	3.99	1.46
43/26b-10	N	Off edge of 3D	-23.93	0.0
43/21-1	Y	Seismic pick updated	5.48	0.0
43/21-2	N	On edge of data gap	132.91	0.0
43/21-3	Y		2.96	0.0
43/21b-5	Y		1.26	0.0
43/26a-8	N	Far outside 3D area	195.07	0.0
43/26b-9	N	Far outside 3D area	71.96	0.0
43/27-3	N	Just off 3D area	182.55	0.0
43/28a-3	N	Outcropping well	30.75	0.0

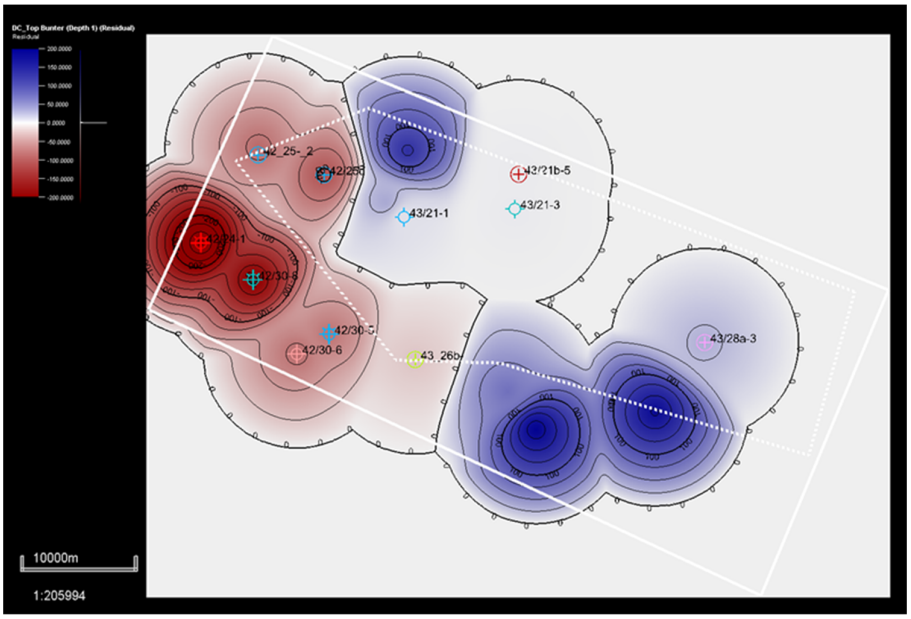

Figure 39 - Map view of mis-ties at Top Bunter Sandstone. A clear W–E trend is observed suggesting a more complex overburden than is currently modelled.

8.0 Geophysical Interpretation Inputs for Subsurface Modelling

The geophysical interpretations described above were used as inputs to subsurface models of the Endurance structure. After depth conversion, the interpreted and well-tied horizons, such as the Top Bunter Sandstone (top reservoir) and Top Bunter Shale (base reservoir) were used to build the static model grid (see Geological Model KKD). The horizons and the fault interpretations were also used as inputs for the geomechanical model (see Geomechanical Model KKD).

8.1 Structural Uncertainty: Upside and Downside Scenarios

To frame the structural uncertainty of the reservoir model grids, a simple approach was undertaken to define upside and downside cases. The southern flank and eastern half of the structure are poorly constrained by wells, so the dip of the southern flank and the thickness of the reservoir in the eastern part of the structure were varied. All ties to wells were kept true in this process, only varying areas with no well coverage (**Figure 40**). The southern flank structure was varied by a +/- 3% error which was applied to the dark red area (**Figure 40**) and then gradually reduced to the outer red dotted line to produce a smooth result. The thickness uncertainty was applied cumulative to the structural dip uncertainty. Given the variations in reservoir thickness observed in wells and the interpretation uncertainty discussed above this was given a +/- 40m error which was applied to the Top Bunter Shale (base reservoir) only. The structural variations did not have a large impact, which can be seen in the limited variation in positions when comparing the upside, base and downside of the spill points (Figure 30). The thickness variations have a larger impact on the gross rock volume (GRV), although this

upside is considered to be realistic given the much thicker sandstone (>300m) observed in the wells immediately south of the eastern half of the structure (43/28a-8, 42/30-5, 43/26b-10, 42/30-6: **Table 10**). The final top and base reservoir upside and downside surfaces are shown in **Figure 41**, **Figure 42** and **Figure 43**. The upside and downside structural surfaces were provided as inputs to the TDRM™ uncertainty modelling in the dynamic model (see Dynamic Model KKD).

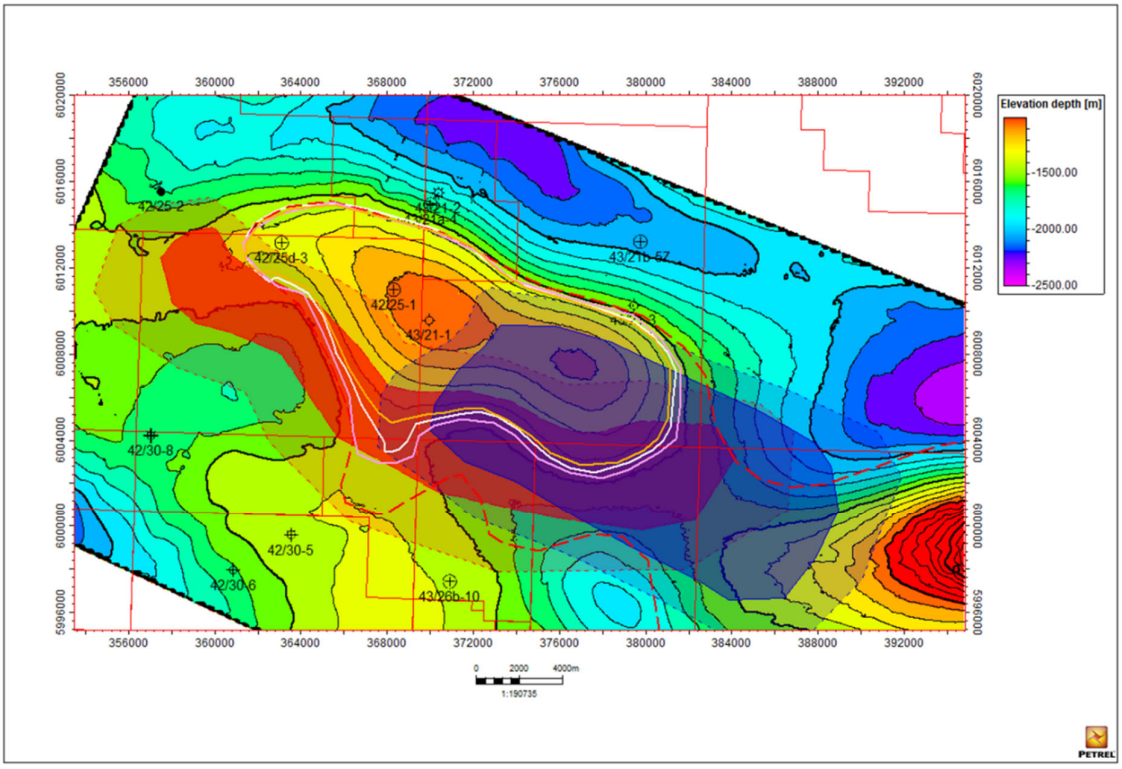

Figure 40 - Dip uncertainty (red) and thickness uncertainty (blue) polygons overlain on Top Bunter Sandstone depth map. The darker polygon shading indicates the area of maximum change which is then gradually reduced to the outer dotted line. The spill points for the upside (pink), base (white) and downside (orange) are also shown. These are cropped at the SPR (red line, broad dashes) in the west where well data indicates very low porosity due to complete halite cementation.

Table 10- Bunter Sandstone thickness in surrounding wells.

	Bunter Sandstone Thickness (m)
42/23-1	189
42/24-1	183
42/25d-3	224
42/30-6	350
42/30-8	230
42/25-2	200
43/21-1	248
43/21a-4	236
43/26b-9	212
43/26b-10	310
43/27-3	289
43/28-1	303
43/28-2	285
43/21-3	232
42/30-5	336
43/21b-5Z	232
43/26a-8	302

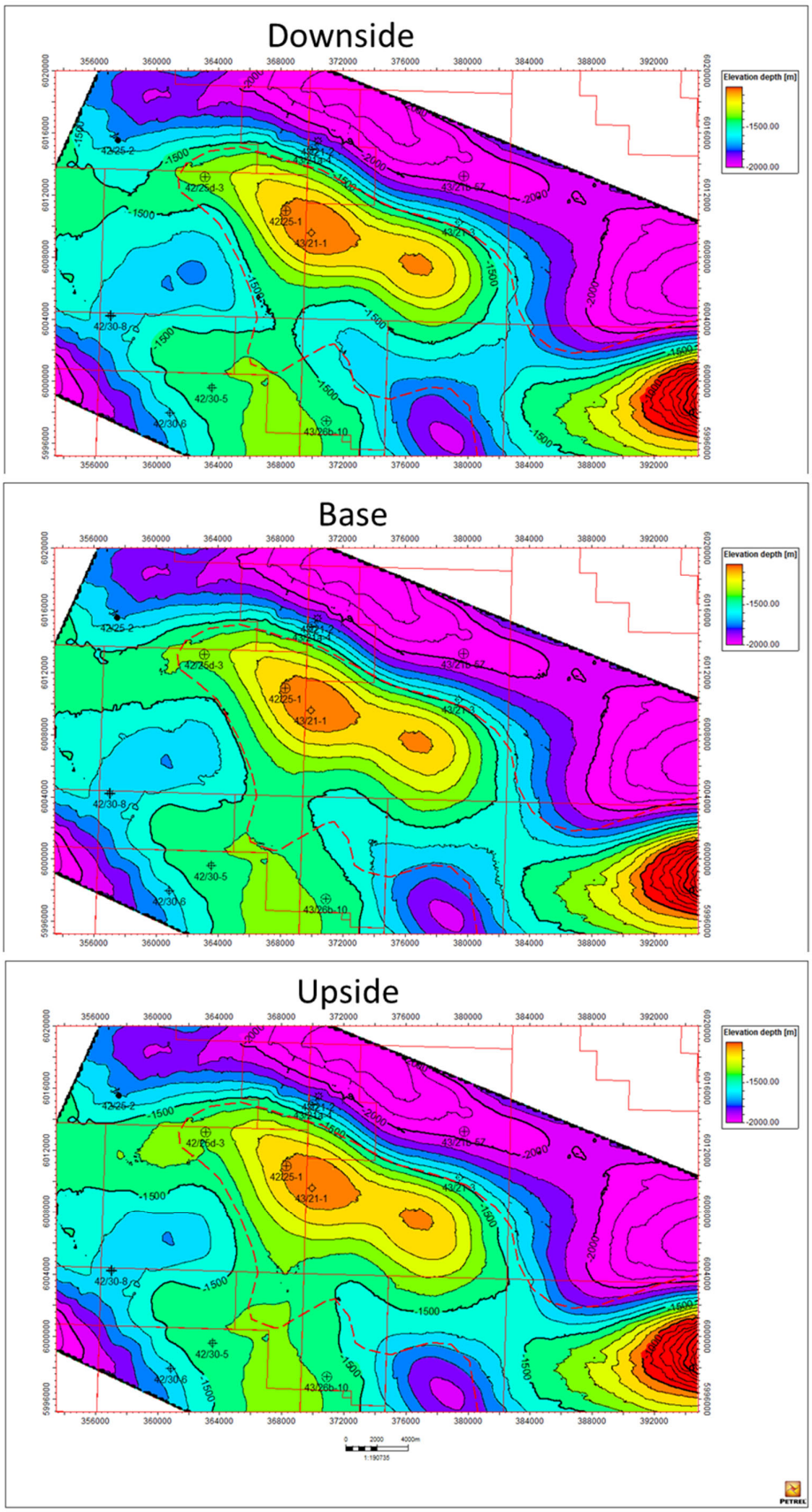

Figure 41 - Top Bunter Sandstone upside, base and downside depth maps.

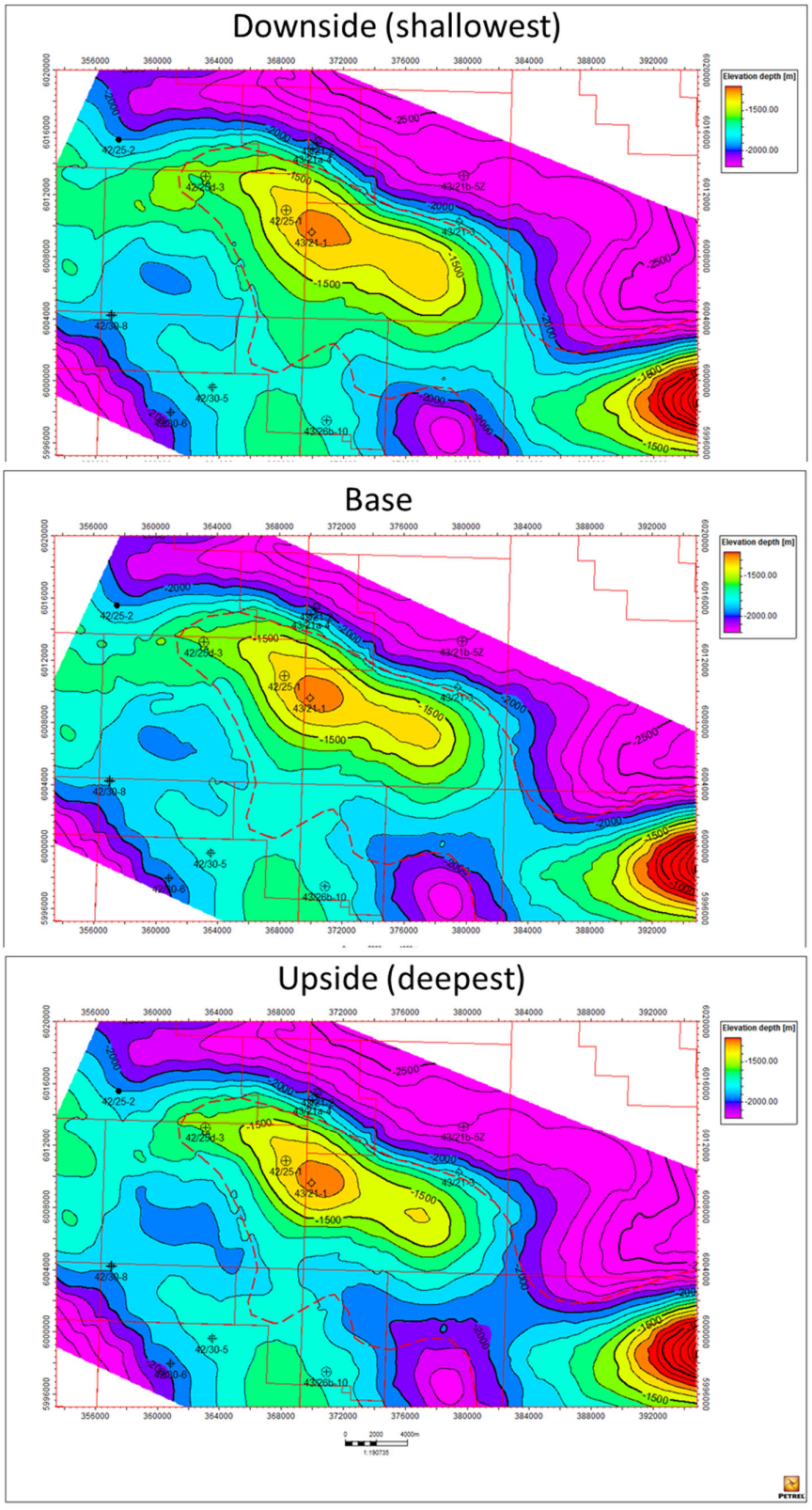

Figure 42 - Top Bunter Shale upside, base and downside depth maps.

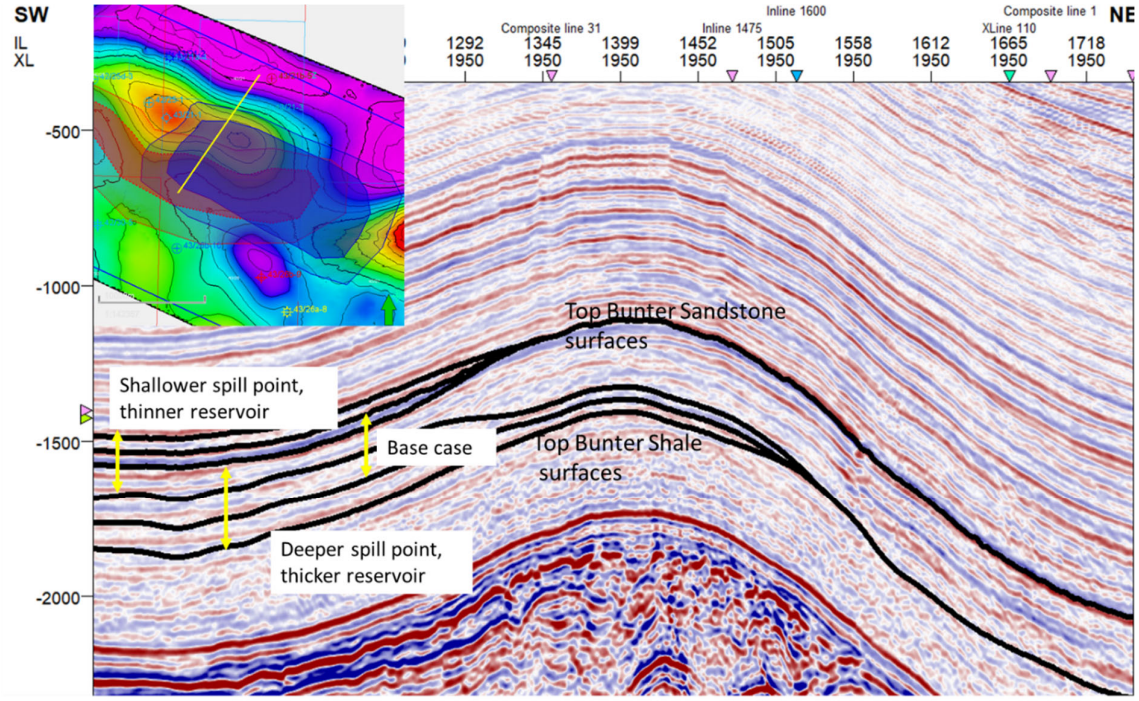

Figure 43 - Upside and downside structural surfaces in section view (seismic in depth).

8.2 Fault Transmissibility

The interpreted fault lineament map at the Top Bunter Sandstone (**Figure 36**) is highly uncertain, and not meant as a definitive map of the locations of faults in the Bunter sandstone. Instead, it can be used to test the impact of faults in the reservoir model.

8.2.1 Modelling Approach

By treating the faults as vertical baffles, the transmissibility of cells which are intersected by fault lineaments can be varied, to test the impact of baffles or barriers on flow. Confidence values were assigned for each lineament to select which faults are included in certain cases.

8.2.2 Transmissibility Modifiers

Given the high net to gross, and broadly high porosity and permeability of the Bunter Sandstone reservoir, fault rocks within the Bunter Sandstone are expected to comprise cataclasites, rather than phyllosilicate fault rocks (Fossen et al, 2018). Fault zones are likely to consist of relatively narrow zones of deformation bands, which form by grain reorganization and crushing (**Figure 44** and **Figure 45**). Shear-enhanced compaction bands (SECB) and pure compaction bands (PCB) only occur in contractional regimes, so the fault rock types expected at Endurance range from compactional shear bands (CSB) to fault core cataclasites. The effect of this reorganization and crushing is two-fold. Pore throats become smaller, and deformation bands can become highly cemented. The degree of cementation likely has the largest impact on permeability and is highly uncertain as no samples of deformation bands exist in the core. **Figure 45** features data from a variety of fault rock types with varying host rock properties.

Whilst the extreme downside is within the range of global data, faults at Endurance are likely to have small offsets and therefore expect a lower degree of permeability reduction compared with larger faults.

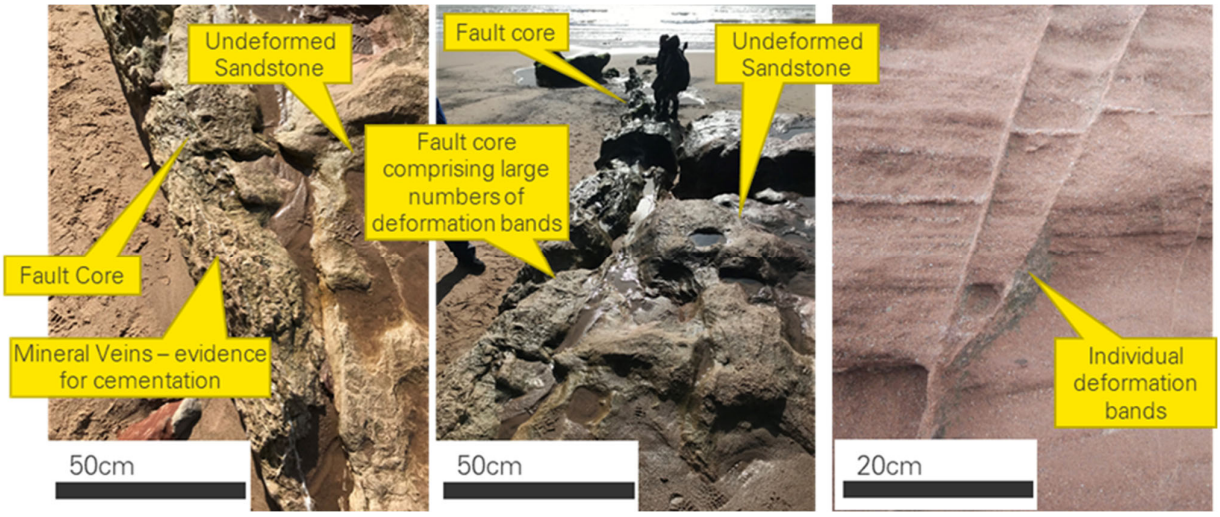

Figure 44 - Images of faults in the Triassic Sherwood Sandstone comprising zones of deformation bands - Exmouth, Devon.

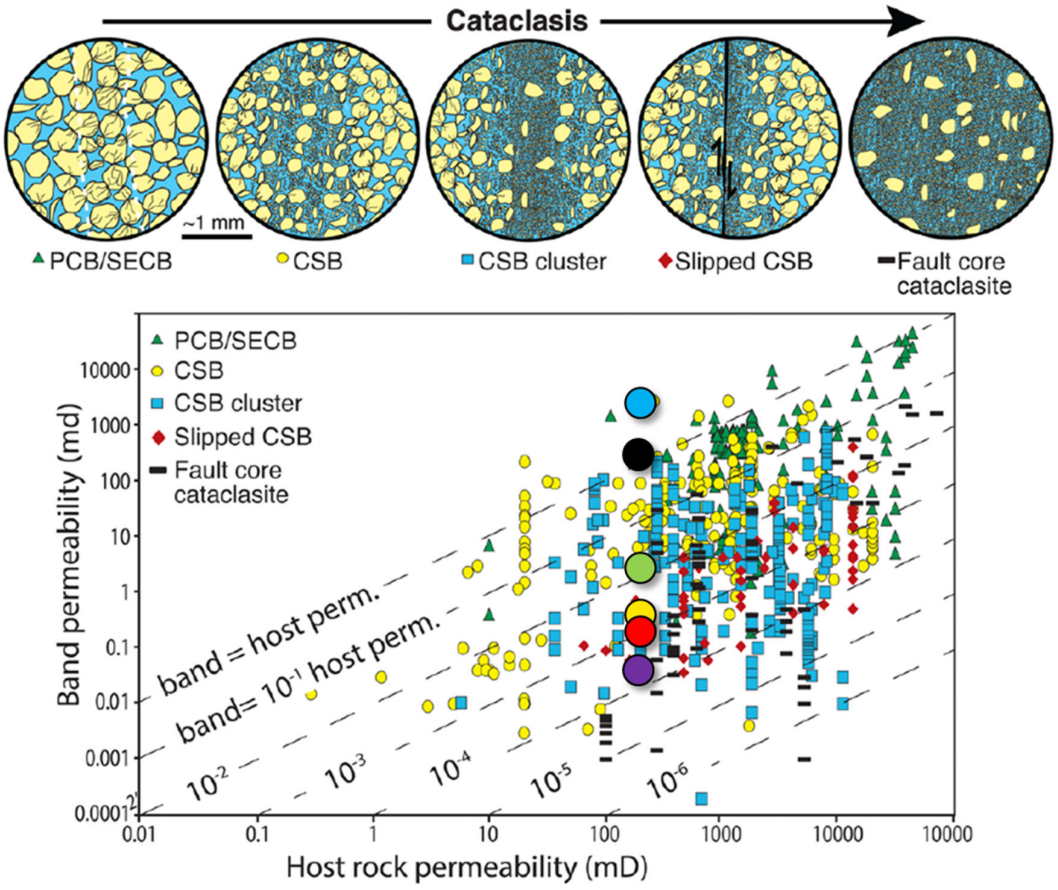

Figure 45 - An overview of deformation band types and effect on permeability (modified from Fossen et al, 2018). Top: degrees of cataclasis and deformation band types. PCB = Pure Compaction Band; SECB = Shear Enhanced Compaction Bands; CSB = Compactional Shear Bands. Bottom: Host rock permeability vs deformation band permeability, overlain with the range of modelled permeabilities from faults used in the TDRM™ uncertainty model. Blue = extreme upside, Black = no fault case, Green = upside, Yellow = mid case, Red = downside, Purple = extreme downside.

The reservoir model transmissibility reduction associated with zones of deformation bands can be estimated using the equation in **Figure 46**. The main controls on transmissibility are the permeability of the host rock, the cell size permeability reduction, fault zone thickness, and grain size and pore throat reduction together with cementation. These parameters lead to typical permeability reduction by deformation bands of between 1 and 5 orders of magnitude, with the most common permeability reduction being between 2 to 4 orders magnitude.

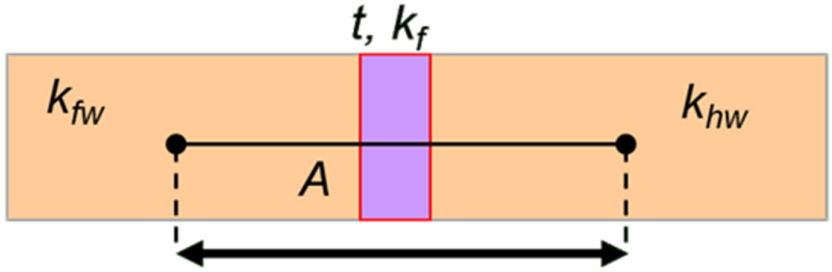

$$TM = \frac{\bar{k}_f}{\bar{k}} = \left(\frac{1}{2k_{fw}} + \frac{1}{2k_{hw}}\right) \Big/ \left(\frac{1-(t/L)}{2k_{fw}} + \frac{1-(t/L)}{2k_{hw}} + \frac{t}{Lk_{fz}}\right)$$

Figure 46 - Approach and equation used to define multiple cases for transmissibility reduction across a fault based on the transmissibility of the grid cell containing the fault, and the thickness and permeability of the fault rock, which is based on a range of models of deformation band development. From bp Reservoir structure toolkit. TM = transmissibility modifier; A & L = grid cell width; t= fault zone thickness; kf = fault zone permeability; k = total permeability; kfw = footwall permeability; khw = hangingwall permeability.

An outcrop analogue was used to define potential fault zone thicknesses (**Error! Reference source not found.**). The outcrop in question, at Exmouth in Devon (SW England), shows two faults in fluvial sandstones of the Sherwood Sandstone Formation – a time equivalent of the Bunter Sandstone Formation (**Figure 44**). The outcrop analogue faults, each with approximately 10m of offset, are about 70 m apart and separated by undeformed sandstone. The faults comprise zones of high-density deformation bands approximately 40 cm wide (though width varies – in places zones are as narrow as 20 cm – **Figure 44**). Based on the lack of seismic evidence of faulting in the Bunter Sandstone Formation at Endurance, the 10m

offset on these outcrop analogue faults is considered consistent with sub seismic faulting that could be expected in the reservoir. It is important to note that while no deformation features were seen in core, the outcrop analogue shows no deformation features between the clusters of deformation bands, so unless wells were drilled through faults, no deformation features would be expected. Based on outcrop analogue, a range of potential fault zone thicknesses of 0.2 – 1.0 m are applied (**Error! Reference source not found.**).

Cell Length	Cell Permeability	Fault Zone Thickness	Fault Zone Permeability Reduction	Fault Zone Permeability	Transmissibility multiplier	Multiplier Chosen?
200	300	Modelled using 4 100 micron aperture fractures per meter			2.0	Transmissible upside
200	300	0.2	100	3	0.90992	Y – Upside
200	300	0.5	500	0.6	0.44494	Y – Base Case
200	300	1.0	1000	0.3	0.16811	Y – Downside
200	300	1.0	10000	0.03	0.01961	Extreme downside?

Using the range of thicknesses, and range of permeability reductions estimated from analogue data, a range of transmissibility modifiers were created using the equation in **Figure 46**. Five cases were created – an upside, base case and downside case for transmissibility modification, and an extreme upside, where faults enhance transmissibility through networks of open fractures and an extreme downside, where the faults are modelled to be close to sealing. Neither of the extreme cases are considered likely. **Error! Reference source not found.** shows the input parameters and output transmissibility modifiers that were provided as inputs to the TDRM™ uncertainty modelling in the dynamic model (see Dynamic Model KKD). The transmissibility values are applied to cells containing fault lineaments.

9.0 4D Feasibility: Seismic Rock Properties

The impact of replacing brine with CO2 in the reservoir was modelled to understand what the seismic response to CO2 injection would be and if this would be detectable. The replacement of brine with CO2 will cause a softening of the rock (decrease in acoustic impedance (AI)) and the increase in pressure from injection will also cause a decrease in AI (**Figure 47**).

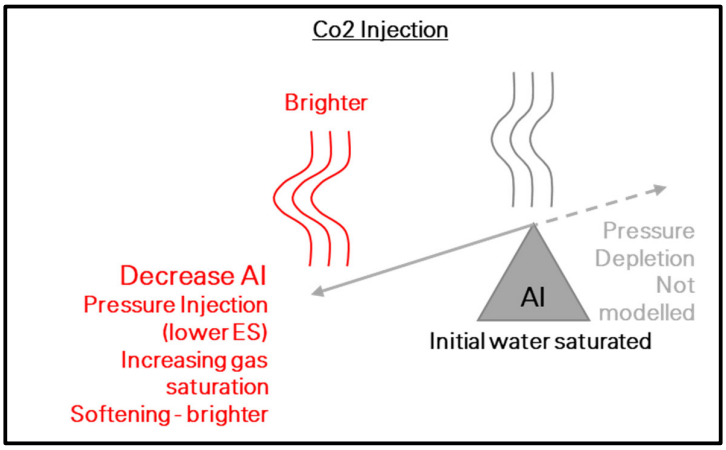

Figure 47 - Basic response to CO2 replacement of brine.

CO2 substitution was carried out for two wells on the Endurance structure, 43/21-1 and 42/25d-3. This work had 3 objectives:

1. To confirm that low CO2 saturations should be detectable at seismic wavelengths
2. To test different wavelets to determine detectability and the impact of seismic acquisition
3. To test a thin bed response to simulate a 'high perm streak' of CO2.

When a small amount of CO2 (2%) is substituted over the injection interval the model indicates that this is already past the AI detection limit (**Figure 48**). Using a wavelet similar to the existing 3D seismic this interval is detected with a trough at the top and a peak at the base.

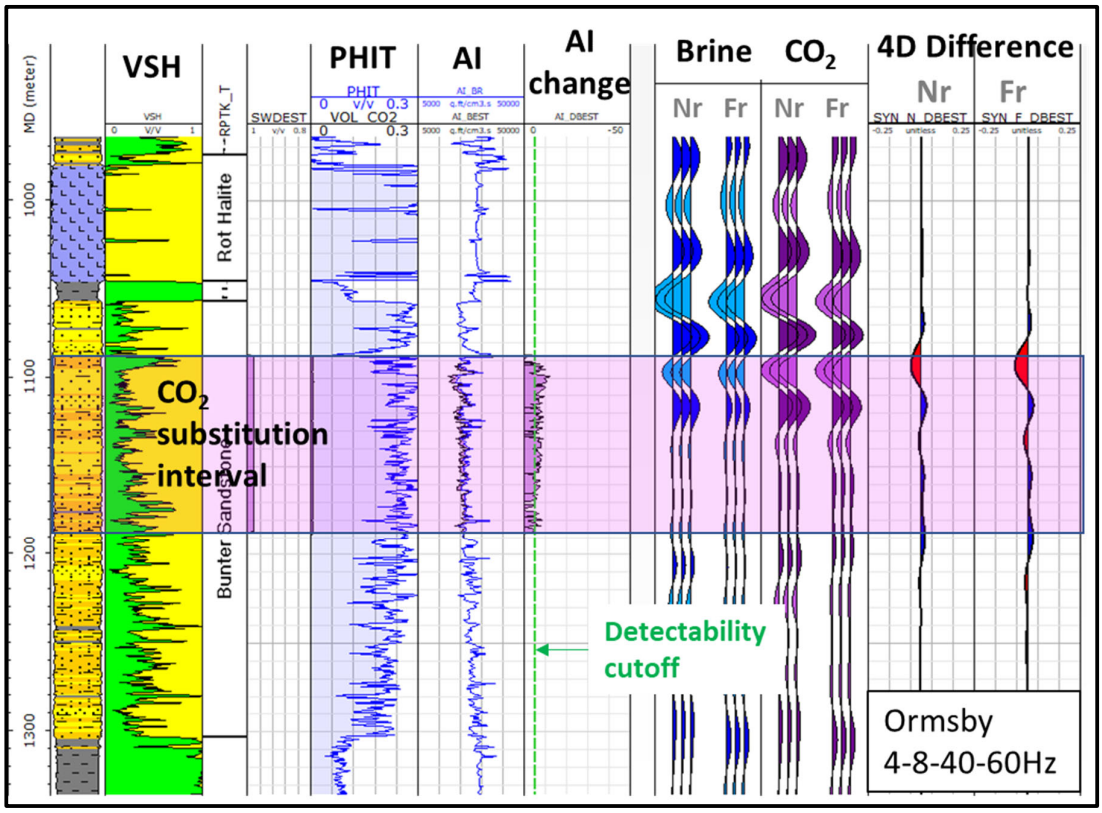

Figure 48- 2% CO2 substituted in injection interval of reservoir at 43/21-1. The top and the base of the injection interval show up in the 4D difference on both nears and fars.

To investigate the impact of the seismic resolution on CO2 detection the CO2 substitution was applied using a porosity cutoff to simulate CO2 only going into the higher porosity/permeability parts of the sandstone. This was done with 3 different wavelets: 4-8-40-60Hz, 8-20-60-100Hz and 10-40-65-180Hz. The results are shown in **Figure 49**, **Figure 50** and **Figure 51**. What is apparent on all scenarios tested is that the resolution of the current 3D seismic would not detect thin beds of CO2. But the higher resolution data would see this. Given the 4D response in **Figure 49**, lower frequency seismic data would likely lead to the interpretation that CO2 was only present at the top of the interval in a layer about 30m thick. This interpretation changes drastically with higher frequency data, which show a 4D response through the whole section. In **Figure 50** the same effect is observed, and even in **Figure 51** when there are very thin layers filled with CO2 the thin streak at the bottom of the zone is detected on the high resolution seismic. This modelling will guide the seismic strategy towards obtaining high resolution seismic for monitoring Endurance during and after injection.

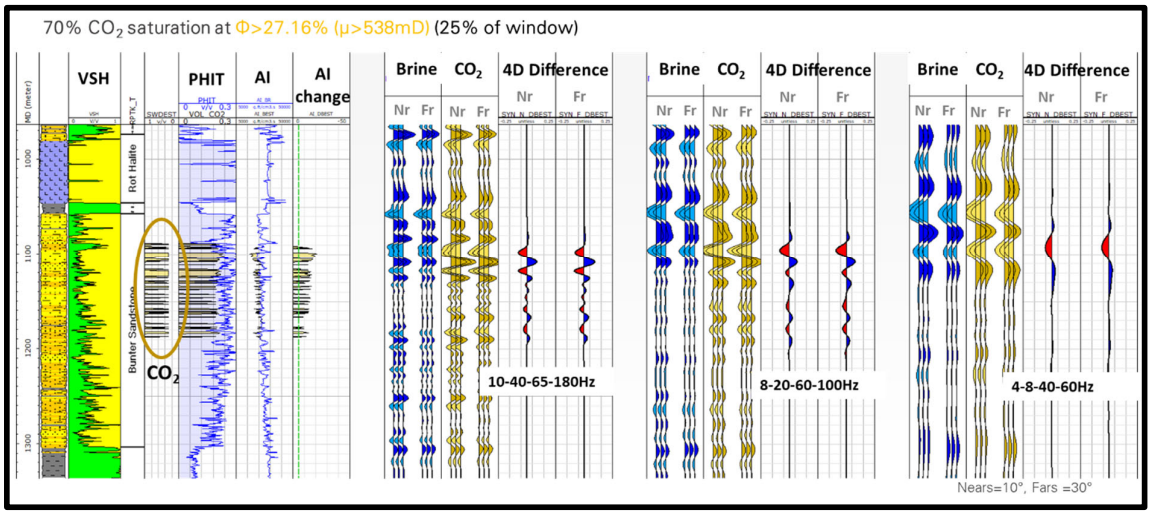

Figure 49 - Filling the 25% highest porosity with CO2.

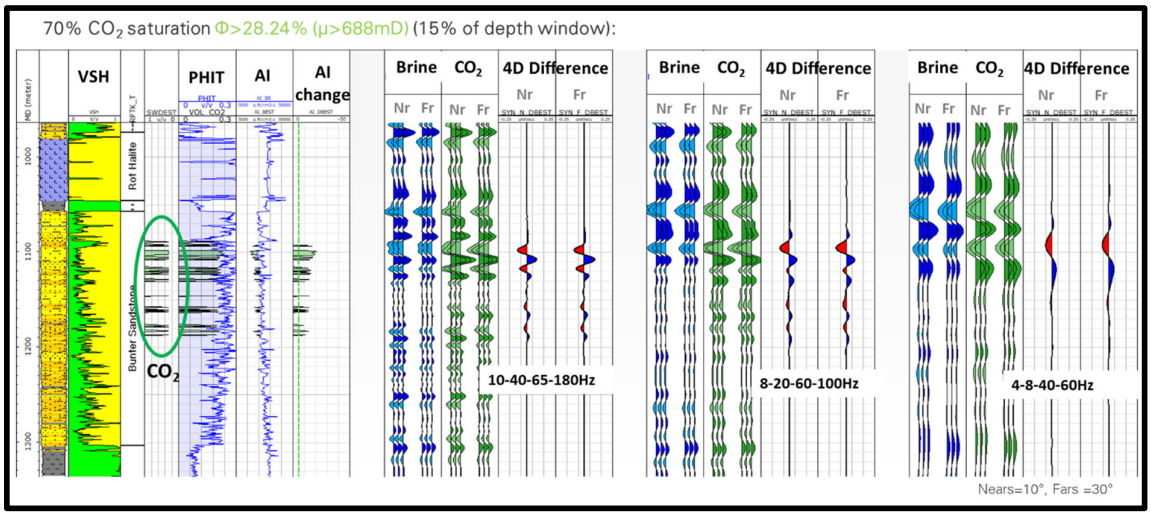

Figure 50 - Filling the 15% highest porosity with CO2.

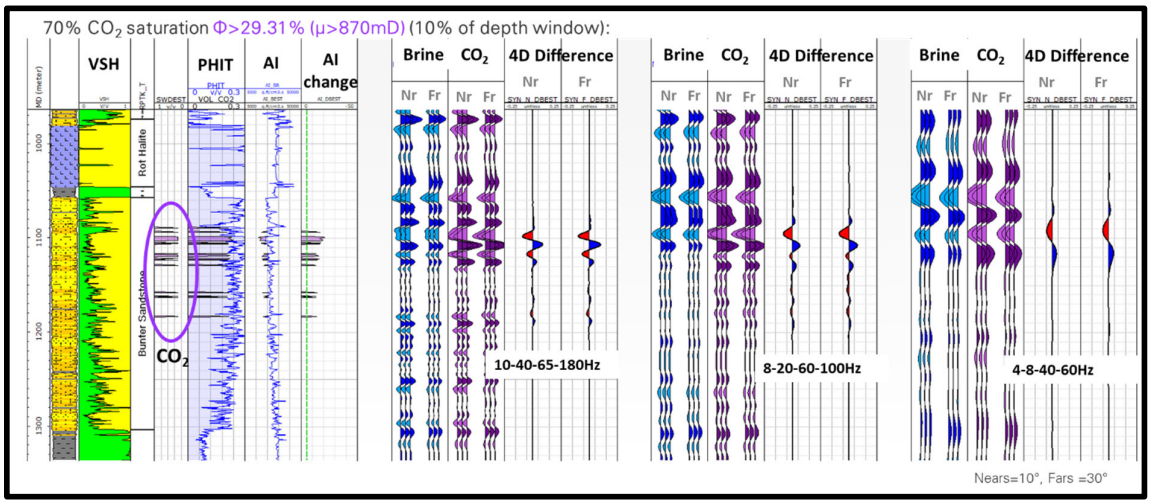

Figure 51 - Filling the 10% highest porosity with CO2.

The 4D seismic modelling under reservoir conditions (taking into account porosity, pressure, and temperature) observed that the 4D response is very large, in the range of 20% change in AI for the crest of the structure in the best quality rock (**Figure 52**) dropping to 8% for the poorest quality rock at the bottom of the Bunter Sandstone close to the spill point. This provides confidence that a 4D seismic response should be easily detectable. **Figure 52** also illustrates that there is very little sensitivity to CO2 saturation: at 20% CO2 saturation there is a 19% change in AI increasing to a 22% change at 71% CO2 saturation (maximum saturation achievable). Therefore, 4D seismic will be excellent for locating CO2 in the reservoir but will probably not provide any information on the amount of CO2 at a particular position, which will therefore have some limitations in overall plume/reservoir monitoring and management.

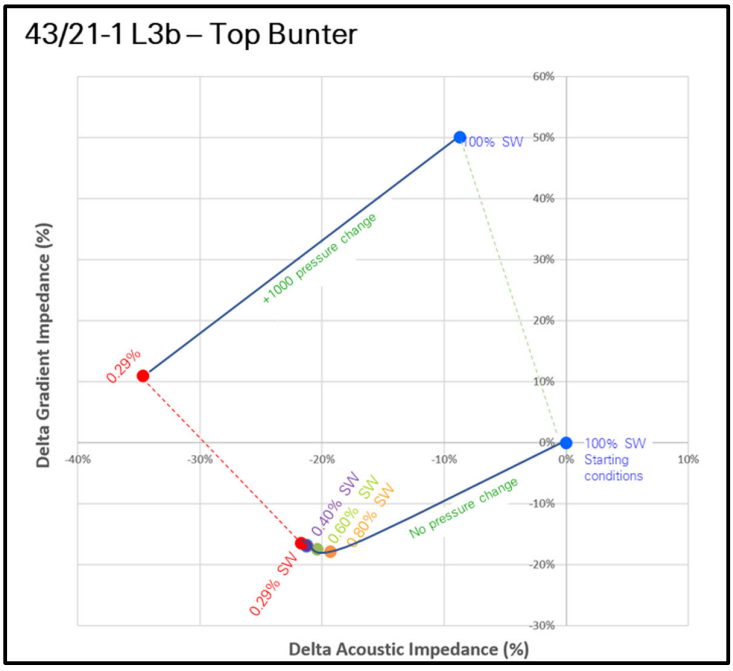

Figure 52 - Change in acoustic impedance (AI) and gradient impedance (GI) with decreasing brine saturation (replaced with CO2) for the high porosity section in 43/21-1.

10 Conclusions

The 1997 OBC 3D seismic survey only covers the Endurance structure and not the outcrop, and whilst the data provide a structural image, it has very low fold in the Triassic section which limits its use for thorough interpretation of overburden and reservoir faulting. The 2013 Polarcus 3D seismic data has higher fold, better overburden coverage and extends east across to the outcrop. The reprocessing of this data for this project significantly enhanced the image quality and reduced the noise within the dataset, enabling improved ability to interpret the horizons and faults in and around the Endurance structure.

Interpretation on the new dataset results in a very similar two-way time structure of Endurance. The Top Bunter Sandstone is a very clear seismic event, and the seismic phase reversal is highly visible in all attributes. However, low impedance contrasts within the reservoir section mean that derivation of seismic attributes for reservoir characterisation has not been possible. The Top Bunter Shale (base reservoir) horizon was additionally interpreted, which had not been possible previously. It is a lower confidence horizon than the Top Bunter Sandstone, but the isopachous nature of the stratigraphy leads to relatively low uncertainty.

The overburden stratigraphy over Endurance is conformable and generally isopachous and the seismic character is very consistent. Reflectors within the Jurassic Lias Group section appear to be parallel to the top of the Zechstein salt, and no evidence of an angular unconformity exists within the Triassic or Lias section. Therefore, the earliest the Endurance structure could have grown was the late Cretaceous, as this is the earliest significant tectonic event after the Liassic.

The new reprocessed 2013 Polarcus 3D seismic data improved the image sufficiently to enable fault interpretation and faults were mapped in the overburden down to a resolution of around 15–20 m vertically. No faulting is observed within the reservoir section on the Endurance structure (no offset at top reservoir or top Permian), although a lack of internal impedance contrasts is challenging for fault identification in this interval. There are still some limitations with the imaging of the shallower 500m at the outcrop location, which introduces some uncertainty into the exact position of the Top Bunter Sandstone subcrop beneath the base Quaternary.

The seismic data and interpretations were depth converted using a simple layered model (V0k), with some modifications due to a lack of suitable seismic velocity cubes. There is some residual uncertainty on the time-depth conversion, which would be best addressed with seismic velocities from reprocessing or new 3D acquisition. The depth converted horizons and faults provided the structural framework input to the static reservoir and geomechanical models, as well as upside and downside scenarios of depth structure and fault transmissibility to test uncertainty.

The existing seismic data, even after reprocessing, is not considered optimal for the Bunter Sandstone at Endurance. It is recommended that new seismic should be acquired focussed on the CO2 store that will have much higher resolution, improved spatial sampling and thorough noise removal. A depth migration will decrease any depth errors in structure and spill point

ahead of well planning. High resolution coverage over the 42/25d-3 appraisal well will also help facilitate well-tie to core and improve seismic reservoir characterisation.

The 4D seismic response from CO2 injection is predicted to be very good. Even at very low saturations CO2 will be detectable, although saturation itself cannot be obtained from seismic. If high resolution seismic data is used for monitoring then even very thin streaks of CO2 should be detectable, which will improve confidence in containment and conformance of the store.

11.0 References

Bachmann G.H., Geluk, M.C., Warrington, G., Becker-Roman, A., Beutler, G., Hagdom, H., Hounslow, M.W., Nitsch, E., Rohling, H.G., Simon, T. and Szulc, A., 2010. Triassic. In: J.C. Doornenbal and A.G. Stevenson (Eds.) Petroleum Geological Atlas of the Southern Permian Basin Area, EAGE Publications, Houten, 149–173.

Conway, A.M. and Valvatne, C., 2003. The Boulton Field, Block 44/21a, UK North Sea. In: J.G. Gluyas and H.M. Hichens (Eds.) United Kingdom Oil and Gas Fields Commemorative Millennium Volume, Geological Society, London, Memoir, 20, 671–680.

Coward, M.P., Dewey, J., Hempton, M. and Holroyd, J., 2003. Tectonic evolution. In: D. Evans, C. Graham, A. Armour and P. Bathurst (Eds.) The Millennium Atlas: Petroleum Geology of the Central and Northern North Sea, Geological Society, London, 17–23.

Doornenbal, J.C. and Stevenson, A.G. (Eds.), 2010. Petroleum Geological Atlas of the Southern Permian Basin Area, EAGE Publications, Houten, 342pp.

Fossen, H., Soliva, R., Ballas, G., Trzaskos, B., Cavalcante, C. and Schultz, R. A., 2018. A review of deformation bands in reservoir sandstones: geometries, mechanisms and distribution. Geological Society, London, Special Publications, 459, 9-33.

Gast, R.E., Dunsar, M., Breitkreuz, C., Gaupp, R., Schneider, J.W., Stemmerik, L., Geluk, M.C., Geisbler, M., Kiernsnowski, H., Glennie, K.W., Kabel, S. and Jones,N.S., 2010. Rötliegend. In: J.C. Doornenbal and A.G. Stevenson (Eds.) Petroleum Geological Atlas of the Southern Permian Basin Area, EAGE Publications, Houten, 101–121.

George, G.T. and Berry, J.K., 1997. Permian (Upper Rötliegend) synsedimentary tectonics, basin development and palaeogeography of the southern North Sea. In: K. Ziegler, P. Turner and S.R. Daines (Eds.) Petroleum Geology of the Southern North Sea: Future Potential, Geological Society, London, Special Publication, 123, 31–61.

Geluk, M., McKie, T. and Kilhams, B., 2018. An introduction to the Triassic: current insights into the regional setting and energy resource potential of NW Europe. In: B. Kilhams, P.A. Kukla, S. Mazur, T. McKie, H.F. Munlieff and K. Van Ork (Eds.) Mesozoic Resource Potential

in the Southern Permian Basin, Geological Society, London, Special Publication, 469, 139–147.

Glennie, K.W., 1997. History of exploration in the southern North Sea. In: K. Ziegler, P. Turner and S.R. Daines (Eds.) Petroleum Geology of the Southern North Sea: Future Potential, Geological Society, London, Special Publication, 123, 5–16.

Grant, R.J., Underhill, J.R., Hernandez-Casado, J. and Barker, S., 2019. Upper Permian Zechstein Supergroup carbonate-evaporite platform palaeomorphology in the UK Southern North Sea, Marine and Petroleum Geology, 100, 484–518.

Guterch, A., Wybraniec, S., Grad, M., Chadwick, R.A., Krawczyk, C.M., Zeigler, P.A., Thybo, H. and De Vos, W., 2010. Crustal structure and structural framework. In: J.C. Doornenbal and A.G. Stevenson (Eds.) Petroleum Geological Atlas of the Southern Permian Basin Area, EAGE Publications, Houten, 11–23.

Ingram, G. M. and Urai, J. L., 1999. Top-seal leakage through faults and fractures: the role of mudrock properties. Geological Society, London, Special Publications, 158 (1), 125-135.

Kombrink, H., Besly, B.M., Collinson, J.D., Den Hartog Jager, D.G., Drozdrewski, G., Dunsar,M., Hoth, P., Pagnier, H.J.M., Stemmerik, L., Waksmundzka, M.I. and Wrede,V., 2010. Carboniferous. In: J.C. Doornenbal and A.G. Stevenson (Eds.) Petroleum Geological Atlas of the Southern Permian Basin Area, EAGE Publications, Houten, 81–99.

Lott, G.K., Wong, T.E., Dunsar, M., Andsbjerg, J., Monnig, E., Feldman-Olszewska, A. and Verreussel, R.M.C.H., 2010. Jurassic. In: J.C. Doornenbal and A.G. Stevenson (Eds.) Petroleum Geological Atlas of the Southern Permian Basin Area, EAGE Publications, Houten, 175–193.

Moscariello, A., 2003. The Schooner Field, Blocks 44/26a, 43/30a, UK North Sea. In: J.G. Gluyas and H.M. Hichens (Eds.) United Kingdom Oil and Gas Fields, Commemorative Millennium Volume, Geological Society, London, Memoir, 20, 811–824.

O'Mara, P.T., Merryweather, M., Stockwell, M. and Bowler, M., 2003. The Trent Gas Field, Block 43/24a, UK North Sea. In: J.G. Gluyas and H.M. Hichens (Eds.) United Kingdom Oil and Gas Fields, Commemorative Millennium Volume, Geological Society, London, Memoir, 20, 835–849.

Pharaoh, T.C., Dusar, M., Geluk, M.C., Kockel, F., Krawczyk, C.M., Krzywiec,P., Scheck-WendeRöth, M., Thybo, H., Vejbaek, O.V. and Van Wees, J.D., 2010. Tectonic evolution. In: J.C. Doornenbal and A.G. Stevenson (Eds.) Petroleum Geological Atlas of the Southern Permian Basin Area, EAGE Publications, Houten, 25–57.

Price, N. J. and Cosgrove, J. W., 1990. Analysis of geological structures. Cambridge University Press.

Richardson, S., 2015. Key structural elements, tectonostratigraphy and lineament analysis of the Southern North Sea. BP internal report, 40pp.

Stewart, S.A. and Coward, M.P., 1995. Synthesis of salt tectonics in the southern North Sea, UK, Marine and Petroleum Geology, 12 (5), 457–475.

Underhill, J.R., 2003. The tectonic and stratigraphic framework of the United Kingdom's oil and gas fields. In: J.G. Gluyas and H.M. Hichens (Eds.) United Kingdom Oil and Gas Fields, Commemorative Millennium Volume, Geological Society, London, Memoir, 20, 17–59.

White Rose, 2016. K40: Subsurface geoscience and production chemistry reports. Capture Power Limited, 300pp., https://assets.publishing.service.gov.uk/government/uploads/system/uploads/attachment_data/file/531045/K40_Subsurface_Geoscience_and_Production_Chemistry.pdf

This publication is available from: www.gov.uk/beis

If you need a version of this document in a more accessible format, please email enquiries@beis.gov.uk. Please tell us what format you need. It will help us if you say what assistive technology you use.